Advanced Drug Delivery Reviews 220 (2025) 115551

Contents lists available at ScienceDirect

Advanced Drug Delivery Reviews

journal homepage: www.elsevier.com/locate/adr

Acoustic tweezers for targeted drug delivery☆

Léa Guerassimoff [a], Stefaan C. De Smedt [a], Félix Sauvage [a,*,1], Michael Baudoin [b,c,**,1]

[a] Laboratory of General Biochemistry and Physical Pharmacy, Faculty of Pharmaceutical Sciences, Ghent University, Ottergemsesteenweg 460, 9000 Ghent, Belgium
[b] Université Lille, CNRS, Centrale Lille, Université Polytechnique Hauts-de-France, Unité Mixte de Recherche 8520, Institut d'Electronique, de Microélectronique et de Nanotechnologie, 59000 Lille, France
[c] Institut Universitaire de France, 1 rue Descartes, 75005 Paris, France

GRAPHICAL ABSTRACT

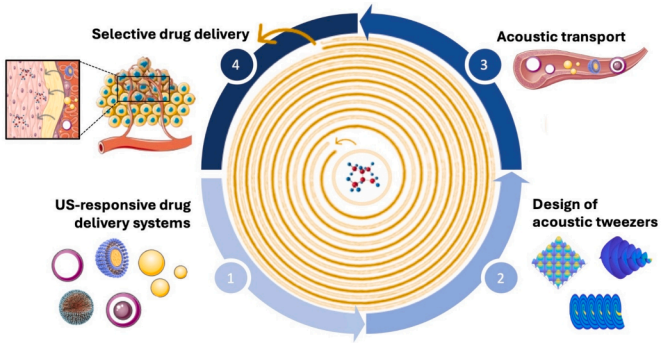

ARTICLE INFO

Keywords:
Acoustic tweezers
Drug delivery
Targeting
Particle trapping
Ultrasounds

ABSTRACT

Acoustic tweezers are a highly promising technology for targeted drug delivery thanks to their unique capabilities: (i) they can effectively operate in both *in vitro* and *in vivo* environments, (ii) they can manipulate a wide range of particle sizes and materials, and (iii) they can exert forces several orders of magnitude larger than competing techniques while remaining safe for biological tissues. In particular, tweezers capable of selectively capturing and manipulating objects in 3D with a single beam, known as 'single beam tweezers', open new perspectives for delivering drug carriers to precise locations. In this review, we first introduce the fundamental physical principles underlying the manipulation of particles using acoustic tweezers and highlight the latest advancements in the field. We then discuss essential considerations for the design of drug delivery carriers suitable for use with acoustic tweezers. Finally, we summarise recent promising studies that explore the use of acoustic tweezers for *in vitro*, *ex vivo*, and *in vivo* drug delivery.

☆ This article is part of a special issue entitled: 'US therapy & imaging' published in Advanced Drug Delivery Reviews.

* Corresponding author.
** Corresponding author at: Université Lille, CNRS, Centrale Lille, Université Polytechnique Hauts-de-France, Unité Mixte de Recherche 8520, Institut d'Electronique, de Microélectronique et de Nanotechnologie, 59000 Lille, France.
E-mail addresses: Felix.sauvage@ugent.be (F. Sauvage), Michael.baudoin@univ-lille.fr (M. Baudoin).
[1] Authors contributed equally.

https://doi.org/10.1016/j.addr.2025.115551
Received 8 August 2024; Received in revised form 15 December 2024; Accepted 19 February 2025
Available online 21 February 2025
0169-409X/

1. Introduction

A major challenge in the drug delivery field is to effectively target and deliver therapeutic agents to their intended destinations. To address this challenge, extensive research has focused on modifying active pharmaceutical ingredients (API) or biological drugs to better control their pharmacological activity and their biological fate. One approach is to develop prodrugs which are APIs conjugated to targeting moieties that can specifically recognize a specific cell receptor. However, they often face rapid clearance and premature degradation in the body [1]. Therefore, the encapsulation of drugs into drug delivery systems (DDS) (e.g. nano- and microparticles) represents a strong alternative by preventing drug degradation and decreasing their clearance by prolonging circulation time in the blood (e.g. through PEGylation) [2]. These advantages over traditional therapies can improve drug targeting to specific sites, delivery of contrast agents for imaging, and overall drug safety [3]. While microparticles (MPs) are mostly employed for sustained drug release [4], chemoembolization [5] or inhalation therapies [6], nanoparticles (NPs) present the advantage of having a smaller size which facilitates their uptake by cells. Controlling the fate of NPs carrying drugs in the body has been made possible by tailoring their shape, surface charge, or modifying their surface with specific ligands that can selectively recognize receptors within the target tissue [7]. However, after injection, DDS generally suffer from poor control over their journey towards the disease site.

When DDS are introduced into the body *via* local or systemic injections, they are subsequently subjected to random motion (Brownian motion) and flow in biological fluids [8]. Efficient delivery to tissues or cells is also impeded by biological barriers (e.g., extracellular matrix, mucus layers, cell membranes) that NPs must bypass to reach their target. To address these challenges, extensive research has been conducted to better control the transport of particles with the aim of improving their accumulation at the disease site. For this purpose, scientists have explored the possibilities offered by external stimuli (e.g., light, magnetic or acoustic fields) to drive drugs to specific locations.

After reviewing existing techniques for externally-driven drug transport, we report here how the unique capabilities of acoustic tweezers for biocompatible remote micro- and nano-manipulation could be combined with specifically designed drug carriers to address previously unmet challenges. The second section compares existing external technologies for the transport of drugs/particles and introduces their respective advantages and drawbacks. The third section introduces the physics behind manipulation with acoustic tweezers as well as the latest developments. The fourth section focuses on the design of suitable drug carriers for acoustic transport. Finally, the last section provides examples of first attempts to use acoustic tweezers for *in vitro*, *ex vivo* and *in vivo* drug delivery and offers perspectives for further exploration of this field.

2. State-of-the-art of externally-driven transport for drug delivery

In this section, we will describe state-of-the-art technologies that are commonly reported in the litterature for moving various particles in the context of drug delivery in order to compare them with the use of acoustic tweezers.

2.1. Light-driven transport

Optical tweezers. Micro- and nano- particles can be manipulated with light using so-called optical tweezers [9]. Optical tweezers rely on the optical radiation forces to manipulate objects with a tightly focused laser beam [10]. Optical tweezers have found many applications in physics and biology ranging from cooling and trapping of atoms [11–15] to the characterization of molecular-scale biological motors [16] and DNA mechanical properties [17], as well as the manipulation of individual cells and microorganisms [18,19]. However, they face several significant drawbacks (see Table 1) that impede their application to drug delivery: (i) the poor penetration of light in opaque tissues limits their use to superficial or transparent tissues and *in vitro* applications, (ii) the force that can be applied by optical tweezers is typically restricted to the piconewton (pN) range [10], which limits their efficiency in counteracting biological flow forces or enabling NP penetration, and (iii) their biocompatibility is constrained by photothermal damage and phototoxicity [20–24].

Opto-thermophoresis. The use of light has found applications in photothermal or photodynamic therapies for cell death induction and triggered drug delivery for spatiotemporal controlled release of drugs [25]. It has also been investigated for displacing particles [26] or cells [27] mostly through thermophoretic motion. In the context of opto-thermophoresis (Table 1), a thermal gradient is created by irradiating a light-absorbing material with a laser at a suitable wavelength to locally increase the temperature. Positive thermophoretic motion, often referred to as 'thermophoresis,' is the phenomenon characterised by the movement of a large molecule or colloidal particle within a solution in response to a macroscopic temperature gradient [28]. Typically, this migration occurs from areas of higher temperature to areas of lower temperature, driven by the increased kinetic energy of solvent molecules in the warmer regions, which effectively propels the colloidal particles towards the cooler side. However, it is worth noting that colloidal NPs can also exhibit an opposite behaviour known as 'negative thermophoretic motion', where they move from "cold" to "hot" regions and accumulate near the focus of the laser, resulting in a form of particle trapping similar to what occurs with optical tweezers [28,29]. The latter is not completely understood but the role of solvent and NP composition strongly affects the direction.

Thermophoresis offers distinct advantages over traditional optical tweezers. Unlike optical tweezers, which rely on differences in refractive indices between colloidal particles and their surrounding environment, thermophoresis is less dependent on such variations. Furthermore, thermophoresis requires lower levels of light power and involves less complex optical setups facilitating potential translation for use *in vivo* [30].

However, there are significant drawbacks that can impede the clinical application of thermophoresis. Firstly, it often involves complex chemistry and necessitates the use of non-biodegradable metals such as gold or platinum. Secondly, as for optical tweezers, light penetration remains limited to a few millimetres to centimetres in the near-infrared, which currently restricts the applicability of this approach to superficial or transparent tissues. Finally, light can be absorbed by biological tissues, leading to photochemical or photomechanical damage to the healthy surrounding tissues as observed in pigmented tissues like the retina [31].

2.2. Magnetically-driven transport

Magnetic nanoparticles have found applications in the treatment of many diseases, including cancer and neurodegenerative disorders [32,33]. These applications harness NPs' ability to induce cell death through heat generation (magnetic hyperthermia), to trigger drug release or to provide magnetic guidance for precise drug delivery.

One key advantage of using magnetic guidance with nanocarriers (Table 1), as opposed to relying on light, is that the human body is essentially "transparent" to magnetic energy and fields [34]. Consequently, magnetic particles, which exhibit greater responsiveness to magnetic fields than tissues, can be subjected to higher localized energy, enabling precise targeting. Therefore, magnetic NPs can accumulate within a region of interest where the magnetic field is applied. Most of the time, superparamagnetic iron oxide nanoparticles (SPIONs) are used as they are magnetised only when a magnetic field is applied, unlike ferromagnetic particles which retain magnetization even after the external field is removed.

Table 1
Comparison of externally-driven modes of transport for drug delivery systems.

Driving field	Technology	Typical size of manipulated particles	Maximal forces	Addressable particles	Compatibility for *in vivo* application	Biocompatibility limitations
Light	Optical tweezers	~100 nm to ~ 10μm	~ 100 pN	Optically transparent or absorbent Preferably with a higher refractive index than the surrounding medium	Limited to superficial or transparent tissues in the visible range Up to a few cm of penetration in the near-infrared range	Thermal damages and phototoxicity induced by the laser
	Opto-thermophoresis	~100 nm to ~ 10μm	~ 100 pN	Contrast in thermal conductivity and specific heat compared to the surrounding medium	Limited to superficial or transparent tissues in the visible range Up to a few cm of penetration in the near-infrared range	Thermal damages and phototoxicity induced by the laser
Magnetic	Magnetic tweezers	~1 μm to 10μm	~ nN	Magnetic and superparamagnetic beads	Only limited by the strength of the magnetic field required for deep penetration into the tissues	Careful choice of magnetic materials and surface coating is required to ensure biocompatibility
Acoustic	Acoustic tweezers	~ 100 nm to mm	~ μN	Particles with density and/or compressibility contrast compared to the surrounding medium	Trade-off between: (i) the spatial selectivity (which increases linearly with the frequency), and (ii) the penetration depth of US (which is inversely proportional to the frequency in soft tissues and thus decreases with the frequency).	No damage produced by the field below cavitation and deleterious heating thresholds. Biocompatible and biodegradable materials must be chosen among the large range of US-responsive materials

While magnetic guidance holds promise, it also presents certain limitations. As in the case of opto-thermophoresis, relatively complex systems are required since they must incorporate a superparamagnetic component in their structure along with the cargo of interest. Besides, particles cannot be accumulated in 3D as using a magnetic field implies a two-dimensional organisation of the objects which can limit their penetration in the targeted tissue. Finally, it is crucial to consider that patients cannot be exposed to a magnetic field for extended periods of time, which can significantly restrict therapeutic efficacy [35].

2.3. Assets of acoustic tweezers for drug delivery and comparison to other techniques

In comparison to light and magnetically-driven transport, acoustic manipulation techniques are of great interest for drug delivery applications (Table 1) since they enable:

(i) **the manipulation of a wide range of particles' materials** (as long as the density and/or the compressibility contrast of the object is sufficient compared to the surrounding fluid [36]) **and sizes** (from millimetric [37] down to micrometric [38] or even nanometric sizes [39], depending on the driving frequency (typically from MHz to GHz frequencies) and the trapping mechanism at play (i.e. radiation force or acoustic streaming, see **section 3.1**).

(ii) **the application of higher forces** magnitude (up to μN [40]) compared to their optical or magnetic counterparts. This capability is essential for controlling drug carriers, delivering drugs in strong flow environments and overcoming biological barriers.

(iii) **high biocompatibility** below cavitation and deleterious heating thresholds defined by the mechanical and thermal indices.

(iv) **non-invasiveness with good penetration of ultrasounds (US)** into human tissues. Note that the penetration depth relies on the driving frequency, as detailed in **section 3.1.**

(v) **strong spatial selectivity** (i.e. the ability to target and move a specific object independently of other neighbouring objects) **and 3D trapping capabilities** since the acoustic wavefield can be engineered to obtain 3D localised traps [40–42].

(vi) **ease of synthesis** as the appropriate wavefields can be synthesised with recently developed holographic techniques, see **section 3.3**.

Table 1 summarises the possibilities and limits of the main manipulation techniques (i.e., magnetic field, light and acoustics) from the perspective of *in vivo* drug delivery. In **section 3** the underlying physics of acoustic manipulation with acoustic tweezers will be described with a special focus on how acoustic tweezers can be designed for drug delivery applications. After the description of drug delivery systems suitable for acoustic manipulation (**section 4**), we introduce existing results on drug delivery with acoustical techniques in the last section (**section 5**).

3. Acoustic tweezers: Principles and capabilities

The effective *in vivo* manipulation of DDS for therapeutic applications requires a comprehensive understanding of their interactions with acoustic waves. In this section, we will (i) introduce the fundamental physical principles underlying the acoustic manipulation of particles and fluid with acoustic waves and their consequence on the design of appropriate DDS, (ii) explain how the field can be shaped to manipulate DDS for targeted drug delivery, and (iii) discuss the capabilities and limitations of current acoustic technologies envisioned for relevant wavefields synthesis.

3.1. Physical principles

Acoustic waves are defined as small vibrations propagating through a supporting medium. They are generally divided into infrasound (frequencies below 20 Hz), sound (between 20 Hz and 20 kHz), and ultrasound (above 20 kHz), depending on how the frequency content of the wave compares to the audible spectrum. To operate at the millimetre down to micrometre length scale in liquids, ultrasounds in the MHz to GHz range are required. At these frequencies, the vibrations are extremely small (typically on the nanometer scale) and fast (over 1 million vibrations per second). In the absence of nonlinearities, the net effect produced by a sinusoidal acoustic wave on an embedded object would be null, meaning that the object would return to its initial position once the wave has passed through it. Hence, the manipulation of objects

with acoustic waves can only be achieved through the use of nonlinear cumulative effects (i.e., effects that are not null when averaged over time).

Two nonlinear effects can be used for the manipulation of particles with acoustic waves [36]: (i) the *acoustic radiation force* and (ii) the *acoustic streaming*. The *acoustic radiation force* represents a net force applied at the interface between two media bearing different acoustic properties (i.e., density and compressibility). This force results from the transfer of pseudo-momentum [43] from the wave to the particle and heavily relies on the acoustic contrast between the object to be manipulated and the surrounding medium. The acoustic radiation force is at the heart of trapping and manipulation with acoustic tweezers and has fundamental practical relevance for the targeted manipulation of DDS. The second effect, called *acoustic streaming*, is a flow resulting from the absorption of the acoustic wave by the supporting fluid. Essentially, the energy absorbed by the fluid is converted into a flow. This flow can be directly used to transport DDS in targeted areas by using the drag force, but it can also be detrimental when the desired effect is the acoustic radiation force, as the flow can release particles held by the acoustic radiation force.

It is interesting to note that the ratio of the respective magnitudes of the *acoustic radiation force* and the *streaming drag force* strongly depends on the size of the particle [44,45]. Indeed, Muller *et al.* [44] demonstrated – for boundary streaming – that below a critical radius, the acoustically-induced (i.e., acoustophoretic) motion of particles is dominated by acoustic streaming while above this value, the acoustic radiation force prevails. Furthermore, the acoustic wave frequency plays a fundamental role in the ability to manipulate particles, especially drug carriers under biological conditions *in vivo*. First, the dependence of the absorption coefficient of acoustic waves on frequency follows a power law, with an exponent close to one in soft tissues within the MHz frequency range, and equal to two in water for frequencies up to the GHz range. Therefore, the manipulation distance strongly depends on the frequency. In addition, the ability to manipulate a single object or a small cluster of objects independently of neighbouring objects, called spatial selectivity, requires focusing the energy in the close vicinity of the object [41,42]. As a wave cannot be focused at length scales that are significantly smaller than the wavelength (λ), and since $\lambda = c/f$, with f the frequency and c the sound speed, of the order of 1500 ms^{-1} in water, the selective manipulation of objects at millimetric scales requires using MHz frequencies while the manipulation of micrometric objects requires frequencies in the GHz range. Thus, there is a trade-off between the manipulation distance and the selectivity.

3.1.1. The acoustic radiation force

Manipulating DDS using the acoustic radiation force requires a thorough understanding of the forces they experience depending on both their intrinsic properties and the characteristics of the incident acoustic field. Various types of wavefields can be considered to manipulate particles, and the expression of the radiation force differs significantly among them. Below, we consider three cases: (i) particles moved by standing waves with a wavelength larger than the particle size (the Long Wavelength Regime, LWR), (ii) particles moved by a progressive wave in the LWR, and (iii) particles moved by a wavefield whose wavelength is comparable to or smaller than the particle size, i.e. the Mie regime.

Acoustic radiation force for a standing wave in the long wavelength regime. Standing waves are characterised by absolute amplitude maxima and minima positions that do not evolve in time. They arise from the interference of progressive waves traveling in opposite directions, which can be generated either by opposite transducers or through reflections at boundaries. In 1962, Gork'ov [46] proposed a simple general formula for the radiation force experienced by a spherical particle in a standing wave in the LWR, that is to say when the wavelength λ is much larger than the particle radius a.

Under these assumptions, the acoustic radiation force $\overrightarrow{F_{rad}}$ can be expressed as the gradient of a potential U:

$$\overrightarrow{F_{rad}} = -\overrightarrow{\nabla} U, \tag{1}$$

with $U = V\left[f_1 \frac{<p_{in}^2>}{2\rho_f c_f^2} - f_2 \frac{\rho_f <v_{in}^2>}{2}\right]$, $<f(t)> = \frac{1}{T}\int_t^{t+T} f(t)dt$ the time average of the function f, V the volume of the particle, c_f the sound speed in the fluid, p_{in} the incident acoustic field pressure, v_{in} the incident acoustic field velocity, $f_1 = \left(1 - \kappa_p/\kappa_f\right)$, $f_2 = \frac{3\left(\rho_p/\rho_f - 1\right)}{2\rho_p/\rho_f + 1}$, and ρ_p, ρ_f, κ_p and κ_f the density and compressibility of the particle (index p) and of the fluid (index f), respectively.

This expression shows (i) that the radiation force is nonlinear, as it depends only on the squares of the incident pressure and velocity fields, (ii) that it is proportional to the gradients of the acoustic potential and kinetic energies, and (iii) that the conversion of these acoustic energy gradients into a force increases with the compressibility and density contrasts between the particle and the surrounding fluid, and vanishes in the absence of such contrasts. This implies that only contrasted particles can be manipulated with the radiation force and that higher contrasts will lead to stronger forces.

Further insights into the force experienced by a particle in a standing wave can be gained by considering the simplified expression for the case of a plane standing wave $p_{in} = A\cos(kz)\sin(\omega t)$, with the wavenumber $k = \omega/c$, ω the angular frequency, and z the axis of propagation of the wave. Plane standing waves correspond to standing waves with constant amplitude and phase in planes orthogonal to the propagation axis. While this configuration is somewhat academic, it allows us to capture some essential physics. In this case, the expression of the force reduces to:

$$\overrightarrow{F_{rad}} = Vk\phi_s E_{ac}^p \sin(2kz)\overrightarrow{z}, \tag{2}$$

with c the sound speed, $E_{ac}^p = <p_{in}^2>/2\rho_f c_f^2$ the acoustic potential energy density, and $\phi_s = \frac{5\rho_p/\rho_f - 2}{2\rho_p/\rho_f + 1} - \kappa_p/\kappa_f$, the acoustic contrast factor, which is a function of the ratio of the density (ρ_p/ρ_f) and compressibility (κ_p/κ_f) contrasts.

First, this expression shows that the radiation force applied on a particle scales linearly with the applied acoustic power (acoustic energy density). Second, this expression indicates that this force decreases rapidly with the size of the trapped particle, as it scales with the volume of the particle. Finally, this expression highlights the role played by the acoustic contrast factor ϕ_s. If ϕ_s is positive, the radiation force has the same sign as the function $\sin(2kz)$, i.e. positive above the central node and negative afterwards. Thus, particles are pushed towards the pressure nodes (minima) (Fig. 1). This occurs for particles that are stiffer (i.e., less compressible) and denser than the surrounding fluid. However, if the contrast factor ϕ_s is negative (e.g. for particles that are more compressible and less dense than the surrounding fluid), particles are pushed toward the pressure antinodes (maxima). Therefore, particles with opposite contrast factors have opposite behaviours.

These three major parameters (i.e., acoustic power, particle size, and acoustic contrast factor) have strong implications for the manipulation of DDS. Indeed, DDS characterized by high density and compressibility contrasts are desirable to obtain a strong radiation force. Secondly, as the radiation force decreases rapidly with the size of the particle, small particles (compared to the wavelength) will experience lower radiation force upon the same incident wavefield. Finally, the trapped position inside a standing wave depends on the density and compressibility contrasts between the DDS and the surrounding fluid. Thus, the acoustic wavefield must be designed properly to trap DDS at the desired position.

Acoustic radiation force for a plane progressive wave in the long wavelength regime. For a plane progressive wave (i.e., a uniform wave traveling freely along a specific axis while maintaining constant amplitude and phase across planes orthogonal to that axis), there is no

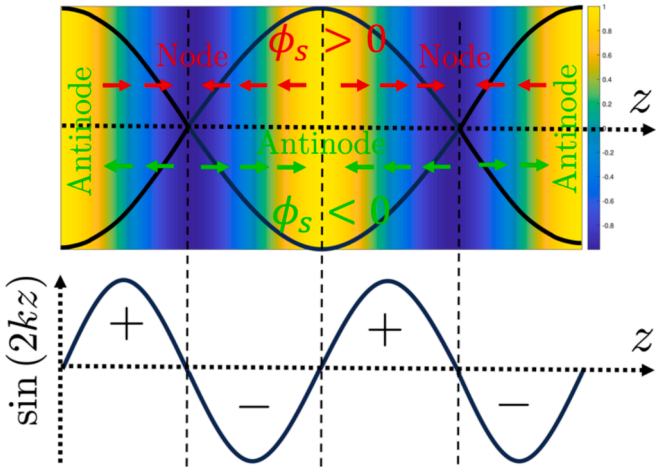

Fig. 1. Graphical illustration of how particles are pushed towards the nodes or antinodes of a plane standing wave depending on their acoustic contrast factor ϕ_s. The background image of the upper graph corresponds to the absolute pressure amplitude, the black lines to the sinusoidal pressure field at two times separated by half a period, and the red arrows and green arrows show in which directions particles are pushed depending on their contrast factor ϕ_s. The graph below shows the sign of the function $\sin(2kz)$, which determines, along with the contrast factor ϕ_s, in which direction the particles are pushed.

gradient of the acoustic potential and kinetic energy, so the Gork'ov's expression of the radiation force vanishes. But this is only due to the limitations of Gork'ov expression, which is not suitable for this type of waves. Gork'ov's expression of the radiation force was later extended by Sapozhnikov & Bailey [46] for any type of incident wavefield (including standing and progressive waves). For a plane progressive wave oriented in the $\vec{z}$ direction their general formulation of the radiation force reduces to:

$$\overrightarrow{F_{rad}} = Vk\phi_p E^p_{ac}(ka)^3\vec{z}, \tag{3}$$

with $\phi_p = 2/3(f_1^2 + f_1 f_2 + 3/4 f_2^2)$

The expression (3) shares some similarities with equation (2) as they are both proportional to the volume of the particle V, the acoustic potential energy E^p_{ac} and the wavenumber k. But: (i) the function ϕ of the density and compressibility contrast differs, and (ii) most importantly, an additional factor $(ka)^3$ appears in equation (3) compared to (2). Since in the LWR, this factor $ka = 2\pi a/\lambda$ is small (since $a \ll \lambda$), the radiation force exerted by a plane progressive wave is some orders of magnitude smaller than its standing wave counterpart. Therefore, when shaping an acoustic field to manipulate small DDS compared to the wavelength, it is noteworthy to underline that if the incident wave is a combination of standing and progressive waves, the standing wave contribution will exert a much stronger force than the progressive one. This expression also shows that the particle is pushed in the direction of propagation of the acoustic wave.

To conclude, the above expressions (equations (1–3)) of the acoustic radiation force relies on several hypothesis: (i) an inviscid fluid, (ii) a harmonic incident wave, (iii) a dilute suspension, (iv) spherical particles and (v) a small particle size compared to the wavelength. Gork'ov's expression of the radiation force has, however, been extended by various authors to account for viscous [47], thermal [48], and transient [49] effects, interaction between particles [50], as well as to treat the case of ellipsoidal particles [51]. These expressions remain nevertheless limited to the LWR. This regime is interesting to transport DDS collectively. Indeed, since particles are small compared to the wavelength in this regime, many particles can experience a similar wavefield and force and hence follow the same trajectory. However, the LWR is limited in terms of (i) *selectivity* (i.e., the ability to target and trap single objects independently of neighboring objects) and (ii) *force,* since the force is directly related to the size of the particle compared to the wavelength.

Acoustic radiation force calculation beyond the long wavelength regime. The calculation of the radiation force applied to a spherical particle, regardless of its size and position, was performed more recently by three groups [46,52,53]. Silva [52] and Baresh, Marchiano, & Thomas [53] developed a multipole expansion method (i.e., the acoustic wavefield was decomposed into a sum of spherical harmonics), while Sapozhnikov & Bayley [46] used an angular spectrum decomposition (i.e., the wavefield was decomposed into a sum of plane waves using a spatial Fourier transform of the wavefield in a source plane). The equivalence of the expressions derived by these different authors was demonstrated in [54]. These methods allow the calculation of the radiation force applied to a particle regardless of its position in the wavefield, enabling the estimation of the stiffness of the acoustic trap created by acoustic tweezers. It is important to underline that when the acoustic wavelength approaches the particle size, some intrinsic resonances of the particle can be excited, leading to trapping forces that can strongly differ (in amplitude and direction) and may even be opposite to the Gork'ov's expression [55]. The regime in which the wavelength is similar to or larger than the particle size, known as the Mie regime, is interesting for the development of spatially selective tweezers capable of targeting single or small collections of DDS, as, in this case, the wavefield can be localized in the vicinity of the DDS by focusing the wave at a length scale comparable to the targeted object. In addition, the radiation force applied to a DDS is much stronger when its size is comparable to the wavelength than in the LWR [55]. Therefore, using the Mie regime is particularly valuable for manipulating DDS in complex environments, such as tissues or flows, where strong forces are required. The force can be further increased by exciting the DDS at its resonance frequency. However, the use of DDS resonances requires highly monodisperse systems as the resonance frequency depends on its size and shape.

3.1.2. *Acoustic streaming*

Origin. As previously mentioned, acoustic streaming results from the absorption of an acoustic wavefield by the medium and from nonlinear effects which convert this absorbed energy into a flow. In standard fluids, the absorption of acoustic waves is due to viscous and thermal dissipation, the former being dominant in liquids. This absorption scales as the square of the frequency in liquid such as water, while the absorption in soft tissues scales as the frequency in the MHz regime, as described previously. The thermo-viscous absorption of the wave can either occur in the bulk of the fluid during the wave propagation but also near the boundaries due to the presence of a thermo-viscous boundary layer. In the first case, the resulting streaming is called "bulk" or "Eckart" streaming, while in the second case, the streaming is called "Rayleigh" or "boundary" streaming.

Boundary or "Rayleigh" acoustic streaming. This type of streaming generates vortices in the vicinity of a vibrating boundary, which can either be a wall, a sharp edge or the surface of a vibrating particle or bubble (Fig. 2).

The first theoretical expression of boundary streaming was derived by Lord Rayleigh [59] in 1884. Since then, boundary streaming has been widely studied in various configurations [56,60,61]. Gradually, models and simulations have been refined to integrate thermal effects [62,63], time dependence [64], larger flow velocities behind the low Reynold number limit [65,66], or even fluid inhomogeneities [67]. Since the computation of the viscous boundary layer is numerically costly, simplified methods based on effective slip velocities have also been developed [68–73].

In the framework of drug delivery, this boundary streaming can be used to generate localised streaming vortices at the extremity of pointy transdermal patches [74] or to create plumes of particles in the vicinity of an oscillating bubble [75], as detailed in **section 5**.

Bulk streaming or "Eckart" acoustic streaming. Streaming flow

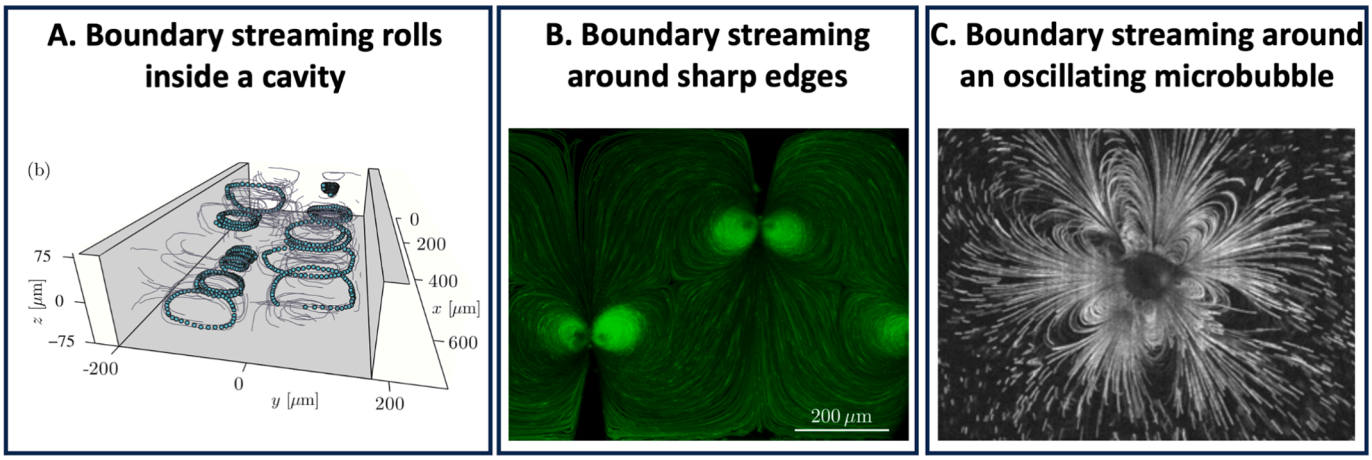

Fig. 2. Illustrations of boundary streaming. (A) 3D measurement of tracers motion induced by Rayleigh streaming inside a cavity. Adapted from [56]. (B) Microstreaming vortices around sharp edges. Adapted from [57]. (C) Microstreaming patterns around a non-spherically oscillating bubble. Adapted from [58].

resulting from the absorption of an acoustic wave in the bulk of the fluid was first reported in the XIXth century [76]. It was then rationalized by Eckart [76,77], who proposed an analytical expression of the flow produced by a plane wave of finite extent insonifying a cylinder by using a vorticity approach. Later on, a simpler expression of the streaming source term that can be readily injected into classical flow equations (i.e., Navier-Stokes) was derived by Nyborg [68] using a time-averaging technique. Nevertheless, while being very simple and theoretically exact, this expression contains terms that do not contribute to acoustic streaming and that can induce large numerical errors, as pointed out in [68,78].

This difficulty was overcome by Riaud et al. [78], who proposed a simple expression for the streaming volumic force $\overrightarrow{f_{str}}$ in a liquid, that does not generate numerical artefacts:

$$\overrightarrow{f_{str}} = \alpha < \overrightarrow{I} > /c_f,$$

where $\alpha = \frac{\omega^2 \mu (\frac{4}{3}+\frac{\xi}{\mu})}{\rho_f c_f^3}$ is the acoustic wave attenuation coefficient, $< \overrightarrow{I} >= < p_{in} \overrightarrow{v_{in}} >$ the time averaged intensity vector, c_f the sound speed in the fluid, ω the angular frequency, μ and ξ are the shear and bulk viscosities of the fluid, and ρ_f its density.

This expression clearly shows that the streaming is proportional to the wave intensity and attenuation. In liquids, the wave attenuation scales as the square of the frequency and increases with the viscosity. Nevertheless, the dependence of the resulting flow velocity on the fluid's viscosity is complex [78], since increasing viscosity enhances the force but also increases the flow resistance. It is important to note that all the aforementioned expressions of bulk streaming were derived under the approximation of laminar (i.e., characterised by low Reynolds number) flows. More recently, researchers have worked on extending bulk acoustic streaming expressions beyond this approximation, both theoretically [79–82] and numerically [83]. Other effects, such as the role played by the near field [84] or the driving frequency [83] on bulk streaming jets have been thoroughly investigated. In particular, it was shown in this last study that (i) small jet radii can only be obtained by increasing the actuation frequency and (ii) the maximum speed of the streaming jet scales as the frequency to the power 3/2, hence offering the possibility to generate extremely high-speed microjets of several metres per second at GHz frequencies, as also reported experimentally [39,85]. In addition to streaming jets produced by plane waves, researchers have investigated the bulk streaming produced by Bessel beams and in particular acoustical vortices [86–89]. They have demonstrated that this type of waves was able to produce a combination of toroidal and poloidal flows.

In the context of drug delivery, bulk streaming appears highly interesting for creating localized jets (Fig. 3) able to transport drugs or particles to a specific location and to help cross biological barriers. The demonstration of precise particle trapping and displacement of microparticles by GHz streaming jets has been demonstrated by Guo et al. [90].

3.1.3. *Implication of the physics on the choice of DDS*

The physical principles introduced in this first subsection have significant implications for the design of DDS. The manipulation using *the acoustic radiation force* requires particles with (i) high density and compressibility contrasts relative to the surrounding fluid and (ii) a significant size compared to the wavelength. Indeed, the magnitude of the radiation force increases with the density and compressibility contrasts and scales with the particle's volume (in the long-wavelength regime, LWR). In contrast, for manipulation using *acoustic streaming*, small DDS (i.e., with a size relative to the wavelength) with low density and compressibility contrasts will be favored as they are minimally influenced by the radiation force and will follow the streaming flow. Naturally, these physical requirements for efficient particle transport must be balanced with biological considerations such as biocompatibility, the ability to cross biological barriers, and the capacity to carry drugs (see **section 4**) to achieve the best compromise for drug delivery applications.

The underlying physics also provides essential guidance in selecting the appropriate wavefield for drug delivery, a topic that will be addressed in the next subsection. Since acoustic tweezers refer to the manipulation of objects using the acoustic radiation force, the next subsection will focus on shaping the acoustic field to optimize the manipulation of DDS with the radiation force.

3.2. *Shaping of the wavefield for DDS transport*

Different types of wavefields have been considered to generate acoustical traps using the acoustic radiation force (Fig. 4).

3.2.1. *Collective manipulation with non-localized standing waves*

First, *non-localized standing waves* have become very popular for patterning [93–100], sorting [101–106], and manipulating objects [107–109] in microchannels. Such standing waves can result either from the interference of progressive waves of the same frequency propagating in opposite directions or from the excitation of cavity mode (Fig. 4***A***). They are of high practical interest for *in vitro* manipulation since (i) microchambers cavity resonances can be used to produce high amplitude standing waves, (ii) the trapping force is some orders of magnitude

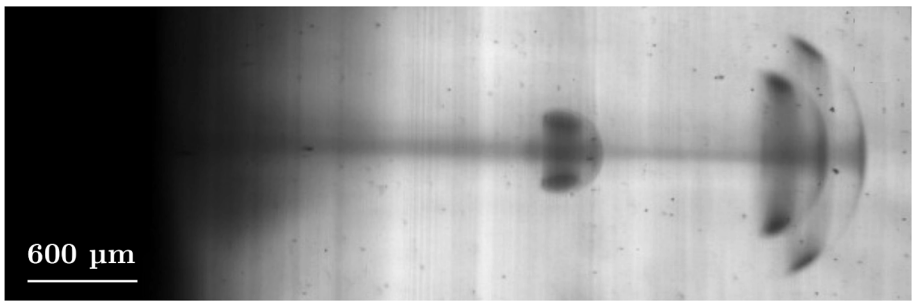

Fig. 3. Image of a bulk streaming microjet produced experimentally with a 750 MHz transducer. The flow is visualised by adding some ink to the water close to the transducer located on the left side. Note that the gravity field is horizontal and oriented toward the left of the picture. Adapted from [85].

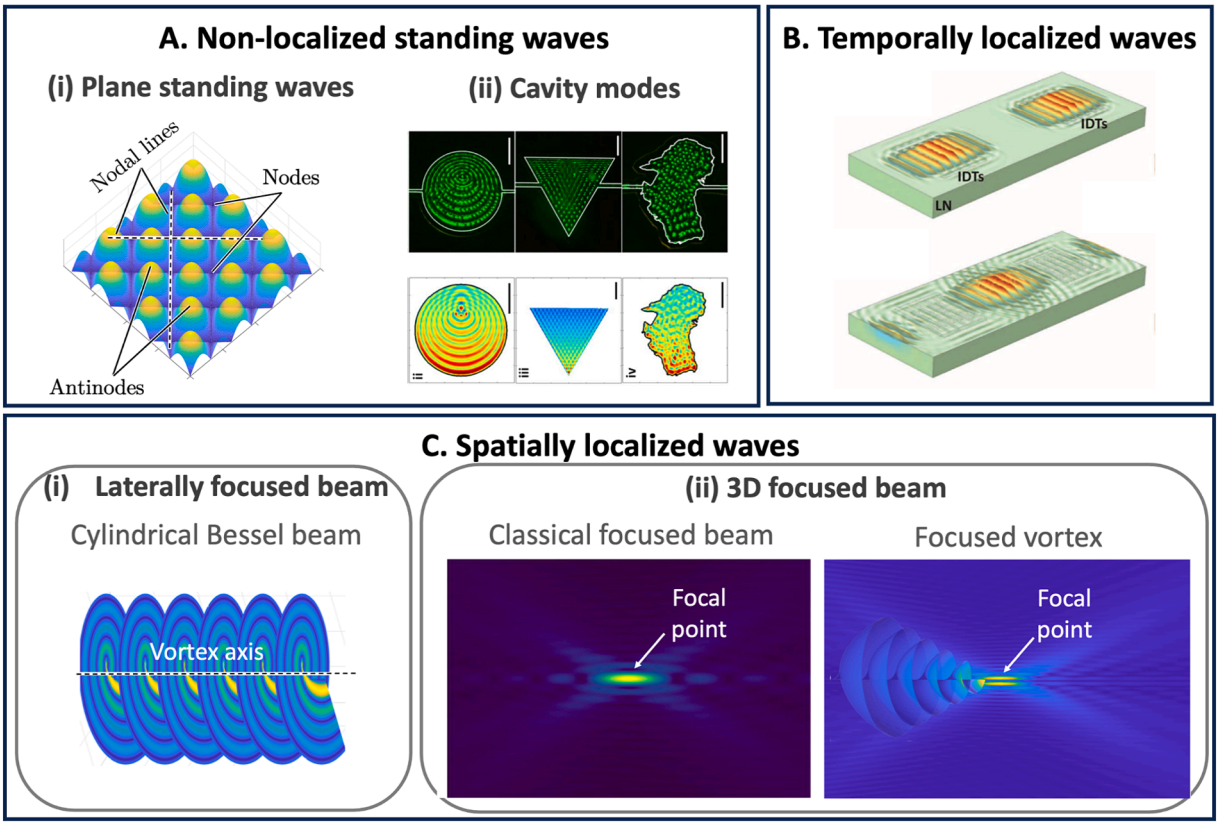

Fig. 4. Common wavefields used for particle trapping with acoustical tweezers. (A) Non localized standing waves: (i) 2D standing wave resulting from the interaction of 2 orthogonal plane waves, (ii) Cavity modes. Adapted from [91]. (B) Temporally localized waves resulting from the intersection of two wave pulses. Adapted from [92]. (C) Spatially localized waves: (i) laterally focused waves (cylindrical Bessel beams), (ii) 3D focused beams (focused wave, focused vortex). Adapted from [36].

larger than the one produced by a progressive wave in the LWR and (iii) particles trapped at the nodes or antinodes of the standing wave can be manipulated collectively. However, they remain of limited interest for *in vivo* targeted drug delivery applications. Indeed, their synthesis would require positioning opposite transducers or a transducer and a reflector all around the area of interest, and that for each dimension of manipulation or to use natural acoustic cavities existing in the human body. Secondly, the wave invades the whole space between the transducer and the reflecting boundaries, resulting in (i) the energy being spread and (ii) the wave collectively affecting all objects along its path, thereby preventing spatial selectivity. Multiple particles trapped at different nodes of a standing wave will consequently follow the same trajectory (Fig. 5***A***). For targeted drug delivery, spatially selective single-beam tweezers are therefore highly desirable to concentrate the energy only in the vicinity of the DDS and hence obtain larger forces, while avoiding side-effects.

3.2.2. *Selective manipulation with localised waves*

Two main approaches have been envisioned to create acoustic traps with spatial selectivity. The first strategy relies on spatial localization through the use of laterally (Fig. 4***B***) or 3D *focused wavefields* (Fig. 4***C***) [40–42,110–114] aiming to localise the energy where the object needs to be trapped. The second approach relies on the use of *pulses* [92,115] that will interact only at a specific location, thus locally generating a trap. Note that the second strategy is not a single beam approach since it requires the interactions between multiple pulses propagating in opposite directions.

Spatial localization with focused wavefields. The use of focused waves to trap objects is at the core of optical tweezers [9]. This idea was then investigated in the field of acoustics early on by Wu [110] and then extensively by Shung and co-workers [111]. But as discussed in **section 3.1.1**, particles that are denser and stiffer than the surrounding medium tend to be trapped at pressure nodes and thus to be expelled from

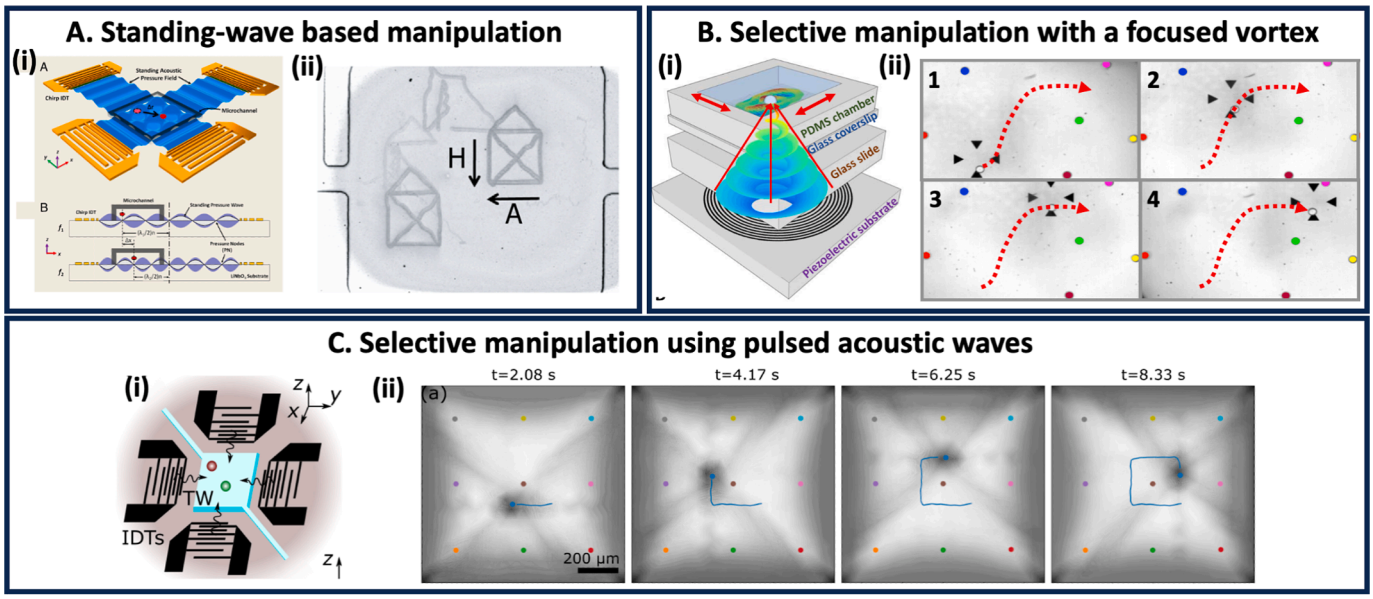

Fig. 5. Illustrations of (A) the absence of spatial selectivity of acoustic tweezers based on non-localized standing waves, and (B,C) the selective manipulation of particles using (B) focused acoustic vortices and (C) pulsed acoustic waves respectively. Spatial selectivity refers to the ability of trapping and manipulating a targeted particle independently of other neighboring particles. (A) (i) Standing wave synthesized using two sets of opposite InterDigital Transducers (IDTs) (see section 3.3). Adapted from [108]. (ii) Image illustrating the absence of selectivity of non-localized standing waves: two particles trapped at two different nodes cannot be moved independently and will follow the same trajectory. Adapted from [107] (B) (i) Representation of a focused vortex generated by interdigitated transducers (see section 3.3) selectively trapping a single particle at the focal point; (ii) Selective displacement of a 75 µm polystyrene bead between other particles using a focused vortex. Adapted from [41]. (C) (i) Two sets of opposite IDTs with large bandwidth used for the synthesis of interacting pulses. (ii) Image sequence showing the spatially selective manipulation of a particle using interacting pulses. Adapted from [115].

pressure maxima in the LWR. Consequently, many particles and microorganisms of interest (e.g., droplets, solid particles, cells, bacteria, etc.), which are denser and stiffer than water cannot be trapped at the focal point of a focused wave (at least in water [116]). This tendency could be modified in the Mie regime. However, an extensive study by Gong & Baudoin [55,116] showed that while it is possible to obtain a 2D lateral trap in water for this type of particles in the Mie regime, (i) this can only be achieved at very specific frequencies close to the particles' resonance frequency, and (ii) no axial trap can be obtained (i.e., in the direction of the wave propagation).

Therefore, an ideal beam for selective particle trapping of this type of particles with a single beam would require a focused beam bearing minimum pressure at the focal point and surrounded by a high intensity pressure shell. This can be achieved by using specific beams called *focused acoustical vortices* [36]. These waves are helical waves spinning around a phase singularity axis. They are called vortices as their phase structure mimics a vortex (Fig. 4***C***). It was first shown theoretically [112] and then experimentally by Baresch, Marchiano & Thomas [40,112] that these vortices exhibit 3D trapping capabilities with a single beam. Selective trappings of micrometric particles [41,42] as well as cells [42] have also been demonstrated with this type of beam in microfluidic chambers (Fig. 5***B***). So far, most of the experimental demonstration of targeted drug delivery using acoustic tweezers relies on this type of beam, as detailed in **section 5**. We can also note that so-called cylindrical Bessel beams can be used to produce a high intensity central beam with only lateral focalisation, if only lateral trapping of the objects is required.

Spatial localization with pulse interaction. This approach relies on pulses generated by opposite transducers interacting locally to create a *localized* standing wave [92,115]. The idea is that, since the acoustic force is much larger for standing waves than for progressive waves in the LWR (see **section 3.1.1**), the two opposing progressive waves will only weakly influence the particles they encounter during their propagation and will strongly affect only those at the points where the pulses interfere. The advantage of this approach is that spatial localization can be achieved using simple, large-bandwidth transducers. The limitations are: (i) selectivity is constrained by the pulse duration, which is itself limited by the transducer bandwidth; (ii) large-bandwidth transducers are less efficient for wave synthesis than their resonant counterparts, thus limiting the amplitude of the synthesized wave; and (iii) this principle mainly works in the LWR, since otherwise other particles would be affected by the propagating pulse, thereby reducing selectivity. Finally, this approach is not a single beam approach and hence requires opposite transducers for each trapping direction, which might be difficult to implement in practice for *in-vivo* targeted drug delivery applications.

The advantages and limitations of the different types of wavefields for drug delivery are summarized in Table 2.

The next natural question is the technology that can be used for the synthesis of appropriate wavefields for DDS manipulation.

3.3. Technologies for the synthesis of wavefields for particles trapping and manipulation

Different technologies can be used to create appropriate wavefields for particle trapping (Fig. 6).

Bulk transducers (Fig. 6***A*).** First, plane waves of finite lateral extent can be generated by simple bulk transducers made of a piezoelectric layer activated by two electrodes deposited on each side of the piezoelectric layer. This transducer can be complemented by a backing layer made of an acoustical absorber to increase the bandwidth to generate pulses. This backing layer increases the bandwidth but at the same time reduces resonance phenomena by absorbing part of the energy, eventually leading to reduced efficiency. It is also possible to insert a quarter wavelength acoustic matching layer to improve the energy transmission to the fluid. These types of bulk transducers can be combined or put in contact with the walls of a cavity to synthesise standing waves. The bulk transducers can also be combined with an acoustic lens to turn the plane wave into a focused wave or a passive hologram to generate a complex wavefield as described below.

Table 2
Comparison of different types of acoustic wavefields for particle trapping and drug delivery.

Type of wavefield	Subtype of wavefield	Spatial selectivity	Trapping capability	Single beam	Type of particle trapped	Radiation force magnitude (+/++/+++)	Advantages for drug delivery	Limitations for drug delivery
Non–localized wave	**Plane progressive waves**	No	No (only pushing)	Yes	No trap	+	Simplicity	Weak force No selectivity No trap (just pushing)
	Plane standing waves	No	1D, 2D or 3D depending on the number of orthogonal pairs of transducers	No	Any	++ (Cavity resonance but energy spread spatially)	Simplicity Relatively strong trap	No selectivity Not single beam
Focused wavefield	**Cylindrical Bessel beams**	Only lateral focusing	Lateral trap (particle pushed along the propagation axis)	Yes	Any (depends on the order of the Bessel beam)	++ (Only lateral focalization)	Strong lateral trap combined with axial pushing	Only lateral trap
	Focused beams	Yes (3D focusing)	3D for specific particles	Yes	3D trap only for particles less stiff and/or less dense than the surrounding fluid	+++ (3D focusing)	Simplicity Selectivity 3D trapping capability Large force	Traps only specific objects Manipulation requires dynamic displacement of the focal point (mechanical motion of the transducer or dynamic field synthesis)
	Focused vortex	Yes (3D focusing)	3D	Yes	3D trap for particles more dense and more stiff than the surrounding fluid	+++ (3D focusing)	Selectivity 3D trapping capability Large force	Manipulation requires dynamic displacement of the focal point
Locally interacting pulses		Yes (local pulse interaction)	1D, 2D or 3D depending on the number of orthogonal pairs of transducers	No	Any	++ (Limited by the transducer bandwidth)	Simplicity Selectivity	Not single beam

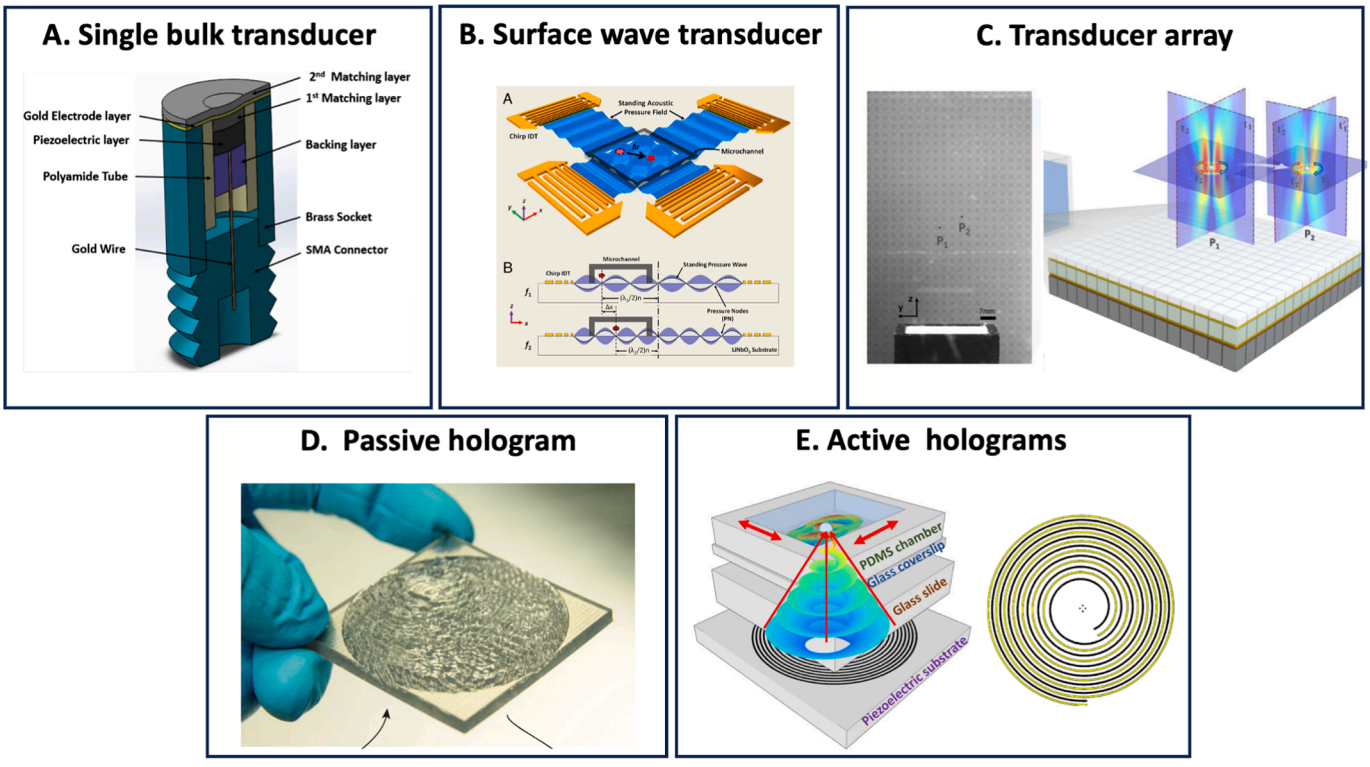

Fig. 6. Figure illustrating different types of technologies used for the synthesis of wavefields. (A) Single bulk transducer; (B) Surface wave transducer; (C) 2D transducer array; (D) 3D-printed acoustic hologram; (E) Interdigital Transducers (IDTs) active holograms. (A),(B),(C),(D) and (E) are adapted from [117,108,118,119] and [41], respectively.

Surface wave transducers (Fig. 6*B*). Surface acoustic waves (also called Rayleigh waves) are waves that propagate along the surface of a solid substrate, with their energy confined within a thin layer—on the order of one wavelength—at the substrate's surface. The most common system used in the literature to synthesize this type of waves in the MHz to GHz range are the so-called Interdigital Transducers (IDTs), some arrays of intertwined metallic electrodes patterned at the surface of a piezoelectric medium. These IDTs were initially used for signal processing in telecommunications [120] but have also been used more recently to trap and manipulate objects in microfluidic set-ups [107–109]. While these surface acoustic waves are extremely interesting for 2D manipulation in microfluidic set-ups (since they are easily transmitted to thin layers of fluids lying above the surface), they appear less interesting for *in vivo* drug delivery applications wherein the manipulation of objects must be performed at larger distances and in 3D. However IDTs have been recently turned into active holograms for complex bulk waves synthesis (see last paragraph).

Transducers arrays (Fig. 6*C*). To generate complex wavefields, a classical method relies on the use of transducer arrays [113,118,121–125]. These transducer arrays enable the synthesis of complex wavefields by controlling the phase and the amplitude of each of the transducers with dedicated electronics. The phase and the amplitude to generate a target signal can be optimised by using the inverse filter technique [126]. The major advantage of these transducer arrays is that the wavefield can be modified dynamically, which means that they could be used to dynamically control DDS. Their main limitations are the price (i.e., the cost of the array and the electronics) and the difficulty in miniaturising 2D arrays to achieve 3D high frequency field control, notably due to cross-coupling, impedance mismatch and microfabrication issues.

Passive holograms (Fig. 6*D*). To address the cost issue, cheaper ways have been investigated to shape wavefields. In particular, many recent investigations have focused on passive approaches to transform a plane wave into a complex wavefield. These passive methods include 3D printed acoustic phase holograms [119,127–131], diffraction gratings [132–134] and metamaterials [135]. These techniques are very convenient as the hologram can be obtained by inexpensive 3D printing or ablation techniques. Nevertheless, the resolution of these cost-effective methods can be limited by the precision of the engraving or printing technique. With this technique, many different types of wavefield including focused waves and acoustical vortices can be synthesized. Even 3D complex wavefields such as wavefields representing a flying bird can be obtained by combining multiple sources [131].

Active holograms based on Interdigitated Transducers (Fig. 6*E*). In the previous approach, the acoustic source and the acoustic hologram are two separate entities. Recently a new approach [41] has been proposed to turn directly the electrodes activating the piezoelectric material into a hologram. This approach relies on the IDTs introduced previously, but this time (i) these IDTs are used to synthesize bulk acoustic waves and (ii) the electrodes are shaped to generate a specific wavefield. This approach has been used to synthesize high frequency focused acoustical vortices for particle [41] and cell [41,42] manipulation. The main advantage relies on its simple fabrication, based on the deposition of a set of metallic electrodes on a piezoelectric medium which can be achieved with high precision by classical photolithography techniques used in the semiconductor industry. This enables the easy synthesis of high frequency complex wavefields for the selective manipulation of small objects [38].

The advantages and limitations of the different types of wave synthesis systems are summarized in Table 3.

4. Drug carriers for acoustics

Building on the fundamental principles outlined above in **section 3**, this part aims to describe DDS that are commonly used in combination with ultrasounds (US) for drug delivery to propose a reflection on which of these systems could be used with tweezers.

While US have been extensively explored for imaging purposes [136], for crossing barriers [137] or for spatio-temporal drug release [138], the use of acoustic tweezers to control the motion of DDS is still in its infancy. In this part, we described existing US-responsive DDS that can be suited for use in combination with acoustic tweezers for controlled-motion while keeping the necessary properties to address drug delivery challenges. We also provide non-exhaustive examples of successful applications of these DDS in combination with US.

4.1. Requirements for acoustic-driven drug delivery

Drug delivery is generally described as the ability to transport an administered compound to a specific diseased tissue or cell, for therapeutic or diagnosis purposes. Conventional delivery of drugs has been carried out using drug carriers, aiming to increase drug stability, pharmacokinetics parameters, safety and delivery efficiency [1391407].

The delivery journey. DDS must overcome three major limitations

Table 3
Comparison of different wave synthesis techniques for particle trapping and drug delivery.

Technology	Simplicity (+/++/+++)	Cost (+/++/+++)	Type of wavefield synthesized	Maximum frequency	Dynamic evolution of the wavefield	Advantages for drug delivery	Limitation for drug delivery
Single bulk transducer	+++	+ (Commercially available)	Plane progressive wave	~GHz	No	Simplicity	Only plane progressive wave can be synthesized with a single bulk transducer
Surface acoustic wave transducer (IDT)	++	++ (Cheap but requires clean room equipments)	Surface wave	~GHz	No	Interesting for on chip operations (*in vitro*)	Not usable for in-vivo drug delivery
Transducer array	+	+++	Arbitrary	~10 MHz	Yes	Strong flexibility for complex manipulation	Cost Complexity Limited frequency => limited selectivity
Passive holograms	+++	+	Arbitrary	Limited by the resolution of the 3D printer or ablation technique	No	Simplicity Arbitrary wavefield => adaptability	Wavefield cannot be modified dynamically Selectivity limited by the resolution of the hologram
Active holograms	++	++ (Cheap but requires clean room equipments)	Arbitrary (but with less precision than passive holograms for complex fields)	GHz	No	Arbitrary wavefield => adaptability	Wavefield cannot be modified dynamically

before reaching the target area: (i) multi-level biological barriers (systemic, microenvironmental and cellular); (ii) biotransformation caused by factors such as pH change, reductive environments and membrane permeation enhancement; and (iii) pharmacokinetic alterations due to factors such as protein binding, blood circulation (shear) stress, drug half-life and clearance. Biological barriers and environmental interactions can significantly affect delivery efficiency depending on the depth of the biological target (e.g. organ, sub-organ and cell) which influence the number of barriers to cross. Therefore, knowledge about *the delivery target* and the *administration route* is crucial when designing DDS. The *delivery target* must be identified in terms of both the drug's site of action, which may occur at different levels (e.g. molecular, subcellular, tissue) and its mechanism of action (e.g. metabolic pathway). Additionally, the *route of administration* must be determined according to the location of the delivery target and the biological barriers that need to be crossed. The *formulation* of the drug carriers must be carefully controlled since their size, surface charge and shape can influence the crossing of barriers (e.g. cellular uptake, sequestration in the extracellular matrix (ECM), endosomal escape), the protein adsorption and their clearance pathway. The choice of the *material* for designing DDS is also of high importance as it can provide sensitivities to external stimuli that could help overcome those three major challenges (i.e., crossing barriers, protein adsorption and body clearance). Indeed, designing DDS with materials responsive to US can help better reach the diseased area through mechanical disruption of barriers or on-site drug release leading to higher delivery efficiency. The material choice also needs to be driven by safety concerns and thus oriented towards biocompatible and biodegradable components such as lipids, FDA-approved polymers (e.g. poly(lactic acid) (PLA), poly(acrylamide) (PAAm)) and proteins.

Two other key factors must be considered especially when designing DDS for use with acoustic tweezers: their ability to release the drug at the targeted location and their acoustic properties.

The release challenge. Once the DDS has reached its biological target, the drug must be released in a controlled and efficient manner. This challenge requires careful design of the DDS, particularly concerning the *drug loading strategy* which can be based on either: (i) covalent linkage or (ii) physical encapsulation. A covalent bond between the drug and the carrier can facilitate the incorporation of stimuli-sensitive moieties [7,141] (e.g., pH, reductive environment or enzymes) enabling drug release in specific areas. However, since covalently-bound drugs can be easily degraded on the surface of the carrier, physical encapsulation emerged as an interesting alternative by providing higher drug stability and improving solubility [142]. The loading strategy also depends on the chemical nature of the drug (i.e. hydrophilic or hydrophobic), as this will influence the choice of material and formulation method. Additionally, not every carrier is suitable for physical encapsulation. For example, microbubbles consist of a thin shell that allows only limited loading capacity around a gaseous core, which cannot be used for encapsulation [142,143].

The acoustic properties. As mentioned **in section 2.3**, acoustic tweezers can trap and displace a large range of particle sizes (typically, from ~ 100 nm to 1 mm) and materials. If the radiation pressure is used as the manipulation force, the drug carrier must have a sufficient acoustic contrast (i.e., density and compressibility) compared to the surrounding medium. However, if the particles are moved based on the acoustic streaming, acoustic contrast is not required. Selective trapping additionally requires the use of particles with sizes comparable to the acoustic wavelength (see **section 3**).

4.2. Capabilities and limits of drug carriers for use with acoustic tweezers

Nano- and microtechnologies have been extensively explored for biomedical applications since the 1960 s and the discovery of liposomes as pharmaceutical carriers [144]. The development of materials for acoustics has revolutionised the perspectives of using US in the biomedical field, paving the way for innovative and transdisciplinary diagnosis and treatment strategies. Various types of polymeric or lipid carriers such as antibubbles, microbubbles, nanodroplets have been designed to meet specific acoustic requirements (i.e., compressibility and density) while also showing promise as systems for drug delivery applications (Fig. 7).

4.2.1. Polymeric systems

Polymeric systems represent promising candidates for designing sophisticated DDS (Table 4 and Fig. 7) due to their ease of synthesis which allows precise control over their size, shape, architecture and charge. Multiple polymer functionalization strategies already exist to improve targeting efficiency, including post-functionalization of hyperbranched polymers [145] or the design of prodrugs [141,145], allowing for either monomer functionalization (*grafting through*), post-polymerization grafting (*grafting from*) or modification of the polymerization control agent (*drug-initiated*) strategies. Moreover, polymers can bypass biological barriers and can be designed to become stimuli-sensitive [146] (e.g., to temperature [147], magnetic fields [148] or pH [149]).

4.2.1.1. Polymeric capsules (i.e., hollow core). Poly(lactic-co-glycolic) acid (PLGA) hollow microparticles have been specifically designed to be responsive to ultrasounds. By evaporating encapsulated materials (e.g., camphor and ammonium carbonate) after the emulsification process, a hollow space is created inside the polymeric particle allowing it to be filled with air. This type of particle has demonstrated significant contrast enhancement (up to 24 and 25 dB when insonated at 5 and 7.5 MHz, respectively [150]). In an effort to improve drug loading which is often complicated by the presence of gas in the inner structure of particles, Kooiman *et al.* have developed oil-filled polymer microcapsules with a shell made of fluorinated end-capped PLA and a tunable core composition for US-mediated delivery of lipophilic drugs. They were able to obtain microparticles with various core types: gas only, a mixture of oil and gas or oil only by adjusting the cyclodecane/hexadecane ratio during formulation. This type of system is highly promising for acoustic-driven drug delivery, as it can encapsulate (i) lipophilic drugs in the oily part inside the capsules and (ii) ultrasound-sensitive gas, offering an alternative to gas-only particles with limited encapsulation capacity. However, special attention must be given to residual solvent traces remaining after formulation, as they may hinder clinical translation [151].

4.2.1.2. Polymeric particles (i.e., plain core). Polymer nanoparticles have also been designed for acoustics using natural polymers like gelatin [152] as a shell component. Interestingly, gelatin can provide sufficient acoustic contrast for high-resolution US imaging. Gelatin-based NPs encapsulating doxorubicin were coated with a high-density peptide layer sensitive to cathepsin B, targeting breast cancer cells that often overexpress this enzyme [153]. The US sensitivity of the gelatin shell enabled real-time monitoring of the nanocarrier transport via videos of the nanoparticle flow in the blood after intravenous (IV) injection in mice.

4.2.1.3. Polymeric fibers (i.e., 3D network). In addition to polymeric particles, nanofibers have also attracted significant attention in the drug delivery field. This system benefits from a large surface area-to-mass ratio, as well as a tunable size (from 1 to 100 nm), diameter and shape [154]. Moreover, post-treatment of nanofibers can allow the formation of a porous 3D network suitable for carrying insoluble drugs. High drug loadings can also be achieved through physical encapsulation within the 3D fiber network by dissolving the drug into the polymer solution prior to electrospinning. However, the amount of drug loading is limited by the solubility and volume of the solvent used [155]. To date, nanofibers have mostly been employed with US for on-demand drug release. Song *et al.* developed nanofibers composed by PLGA and mesoporous silica nanoparticles (MSNs) encapsulating two model drugs:

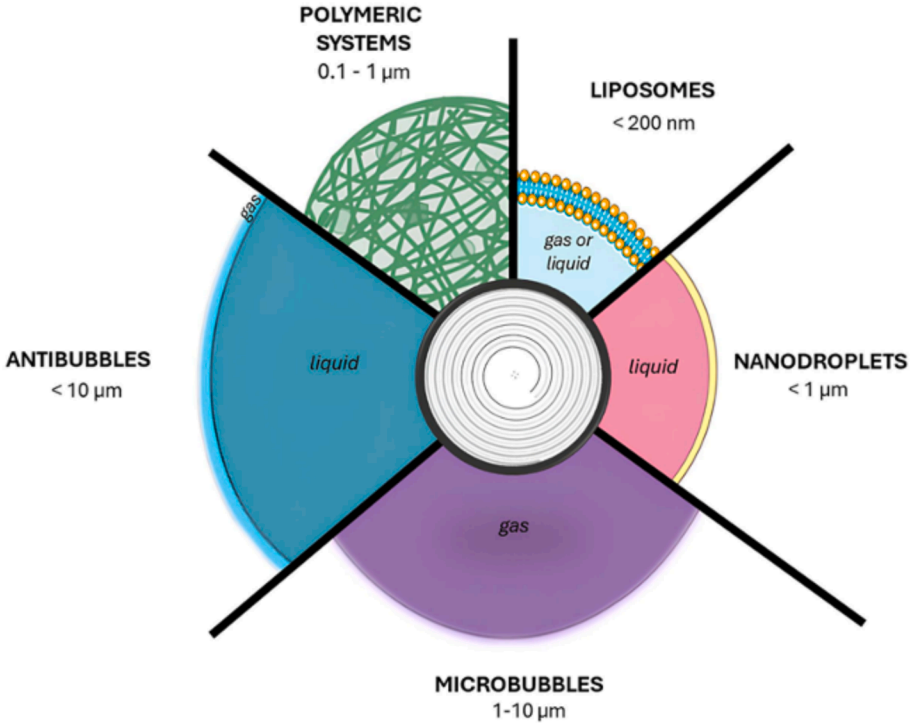

Fig. 7. Overview of the most common drug delivery systems used in combination with ultrasounds.

Table 4
Overview of the capacities and limits of DDS for acoustic-driven drug delivery.

Drug carrier	Average particle size range	Drug encapsulation[a]	Surface functionalization	Acoustic contrast (compressibility, density)	Circulation time	Cell uptake[a]
Polymeric systems	1 nm – 1 µm [211]	+++ [212]	Yes [213]	**Poor** [214] Shell modification [153] Hollow air cavities [150] Mechanophores [159]	**Long** Minutes to few hours [215]	++ [215,216]
Echogenic liposomes (i.e.,gas core)	~100 nm [217]	++ [218]	Yes [219220]	**Medium** Encapsulated gas in the core	**Short** Few minutes [221,222]	+++ [223,224]
Microbubbles	1–10 µm [225137]	+ [226,227]	Yes [228]	**High** Intrinsic gas core	**Short** Few minutes (< 10 min) [191,217,229]	+ [230]
Nanodroplets	< 1 µm [188,231]	+++ [199]	Yes [189,232]	**High** Intrinsic gas shell Phase change for ADV	**Long** Few hours (2–6 h) [191]) [193233]	++ [234]
Antibubbles	1–10 µm [183205]	+ [206]	/[2]	**High** [208] Gas shell rupture Controlled cavitation	**Short** Seconds to min [203]	/[2]

[a] Qualitative evaluation from high (+++) to not yet achieved or demonstrated (–); [2]no data available.

fluorescein (FLU) in the PLGA matrix and Rhodamine B (RHB) in the MSNs. When US were applied for 30 min, a 1.7- and 3.8-fold increase in cumulative release of FLU and RHB, respectively, was observed compared to the non-irradiated group. The authors of this study attributed this enhanced drug release to the temperature increase during US exposure [156]. However, this type of system does not rely on contrast change and cannot be used for US-based imaging or with acoustic tweezers.

4.2.1.4. Site-specific ultrasound-mediated polymer degradation. Site-specific ultrasound-mediated degradation has also been described for controlled drug release through mechanochemical reactions [157]. This approach relies on the presence of labile groups in polymer chains that can be disrupted by mechanical stress (e.g., shear fields, spontaneous

hot-spot generation) during US exposure. It was introduced through the "mechanophore" concept [158] where US irradiation induces conformational modifications in the polymer backbone by applying forces on specific mechanophore groups (e.g. benzocyclobutene, spiropyrans or dicyanocyclobutane) [159]. This can lead to a reduction in chain length and degradation into monomers, making it a promising approach for on-site drug delivery and release. Based on this principle, Li *et al.* designed a mechano-responsive polymeric micellar system consisting of the mechanophore Ferrocene (Fc) conjugated to methoxy poly(ethylene glycol)–*co*-polylysine which dissociates upon US exposure and releases Fe^{2+} and hydroxyl radicals (•OH) in a H_2O_2-rich tumor microenvironment. The authors demonstrated that the release of Fe^{2+} and •OH could induce ferroptosis and inhibit tumor growth in 4 T1 tumor-bearing xenograft mice [160].

Polymeric systems represent promising drug delivery systems for use with acoustic tweezers due to their advantageous properties in terms of: (i) *delivery,* such as high drug loading, surface functionalization with targeting moieties, biocompatibility and ease of synthesis; and (ii) *acoustic capabilities* through the implementation of US sensitivity (e.g., conformational modification) or the incorporation of US-sensitive gas in the core of the NP. However, designing polymeric drug carriers with sufficient acoustic contrast to allow effective manipulation with tweezers remains highly challenging. In this regard, other types of drug carriers have been developed and investigated for acoustic-driven drug delivery such as microbubbles and nanodroplets due to their intrinsically high acoustic contrast but also echogenic liposomes made of a gaseous core.

4.2.2. Liposomes

Liposomes (Fig. 7) have been the subject of intense investigation for decades [144] leading to significant advances in the drug delivery field such as long-circulating PEGylated liposomes, targeted liposomes or dual-drug liposomes for combination therapy. Liposomes consist of a lipid bilayer surrounding an aqueous core. Due to their biocompatibility, stability and ease of production, they are a leading choice for designing drug delivery carriers. However, the rapid clearance of liposomes [161] remains a major challenge despite significant improvements with PEGylation which enhances circulation half-life and reduces opsonization.

4.2.2.1. Liposomes with gas core (i.e., echogenic). Liposomes hold promise for acoustic-driven drug delivery [162] as their structure allows the encapsulation of highly US-sensitive gas (Table 4), enabling the cavitation phenomenon. Cavitation can be divided into two major categories: (i) *inertial cavitation* characterized by the rapid growth and collapse of the lipid bubbles, and (ii) *stable cavitation* which involves the constant motion of the bubble in response to acoustic oscillation (Fig. 8).

Gas-containing liposomes, also called *echogenic liposomes*, are US contrast agents that allow the use of lower intensities, thus reducing the risk of cell and tissue toxicities. They represent promising carriers for drug delivery as they can encapsulate various substances similarly to conventional liposomes, and drug release can be controlled by external US stimuli (i.e., single US pulse at high amplitude, or several low-amplitude US pulses). Besides, the application of US pulses induces cavitation, enhancing tissue or cell permeabilization (i.e., sonoporation) which leads to higher delivery efficiency [162]. The acoustic properties of echogenic liposomes can be optimized by modifying the rigidity of the lipid bilayer through changes in lipid composition and in the nature of the encapsulated gas. The choice of the gas core depends on the targeted liposome size as a higher gas volume results in larger particle size but also in a faster gas diffusion rate in the bloodstream. Rapid gas diffusion and leakage can occur *in vivo* leading to a decrease in the echogenicity of liposomes. Supercritical CO_2 has been used as gas for the formulation of echogenic liposomes [164]. These liposomes have been prepared under high pressure and dissolved CO_2 (i.e., gas-like) has been incorporated reaching a concentration of 1.15 mol/kg at 10 MPa. Furthermore, ionized CO_2 was also encapsulated, using monoethanolamine during the physical process, resulting in a significantly higher acoustic response. A fluorescent model drug was physically loaded into both CO_2-loaded (i.e., dissolved and ionized) liposomes and into conventional liposomes prepared with the Bangham method (Fig. 9***A***). Interestingly, echogenic liposomes led to much higher releases (67–77 %) than liposomes prepared with the Bangham method (4 %) under a current of 0.25 A.

In addition to CO_2, other gases have been loaded into liposomes such as perfluoropropane (C_3F_8). PEGylated lipids have been used to formulate C_3F_8-loaded liposomes [165] in order to increase stealth properties *in vivo* but also to increase their stability by reducing gas diffusion and leakage. A supplementary coating based on 1,2-Distearoyl-*sn*-glycero-3-phosphoglycerol (DSPG) has been added to acoustic liposomes containing 6 mol% of 1,2-Distearoyl-*sn*-glycero-3-phosphoethanolamine (DSPE)-PEG. This coating led to a significant increase in the echogenicity half-life of the liposome (63 min) compared to uncoated liposomes which exhibit a 31 % shorter half-life. This formulation strategy also enhanced the carrier's stability and allowed for a longer imaging period *in vivo* by delaying the exponential decrease in the liposomes' echogenicity compared to standard liposomes (i.e., without extra coating), resulting in half-lives of 56.5 s for the standard formulation and 132 s for the optimized formulation (Fig. 9***B***).

4.2.2.2. Liposomes with a liquid core. Other gases, such as sulfur hexafluoride, have been employed to enhance delivery *in vitro* and *in vivo.* [166]. However, liposomes with a gas core are still often associated with poor stability and a very short half-life in blood circulation (<10 min) after US exposure. To address these issues, new designs of acoustic liposomes have emerged, replacing the gas core with a liquid core to overcome instability caused by rapid gas diffusion and leakage, which requires time-consuming protocols. This approach also had the advantage of relying on mechanical activation without the need of heating at high temperatures and with shorter US protocols. Such US-induced drug release has been based on the acoustic impedance and osmolarity of a liquid phase made of sugars diluted in aqueous buffers [166,167]. Interestingly, the addition of sugars in aqueous buffers has shown to shift the buffer acoustic impedance. The liquid-core liposome was then loaded with the lipophilic drug ketamine (Fig. 9***C***). Drug release studies demonstrated that 5 % and 10 % addition of sucrose in the buffer core led to significantly more ketamine release than without any sugar under

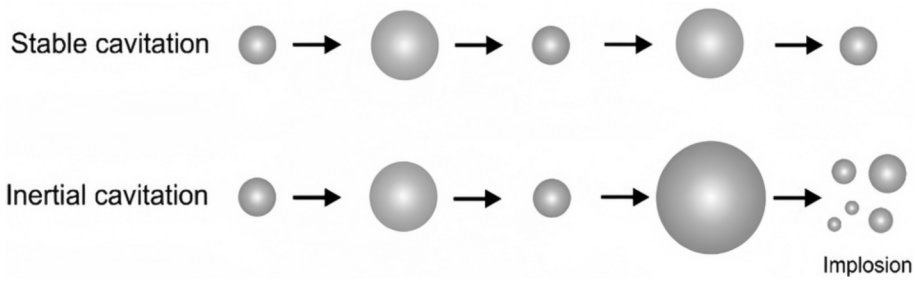

Fig. 8. Description of the two types of cavitation (i.e., stable and inertial). Adapted from [163].

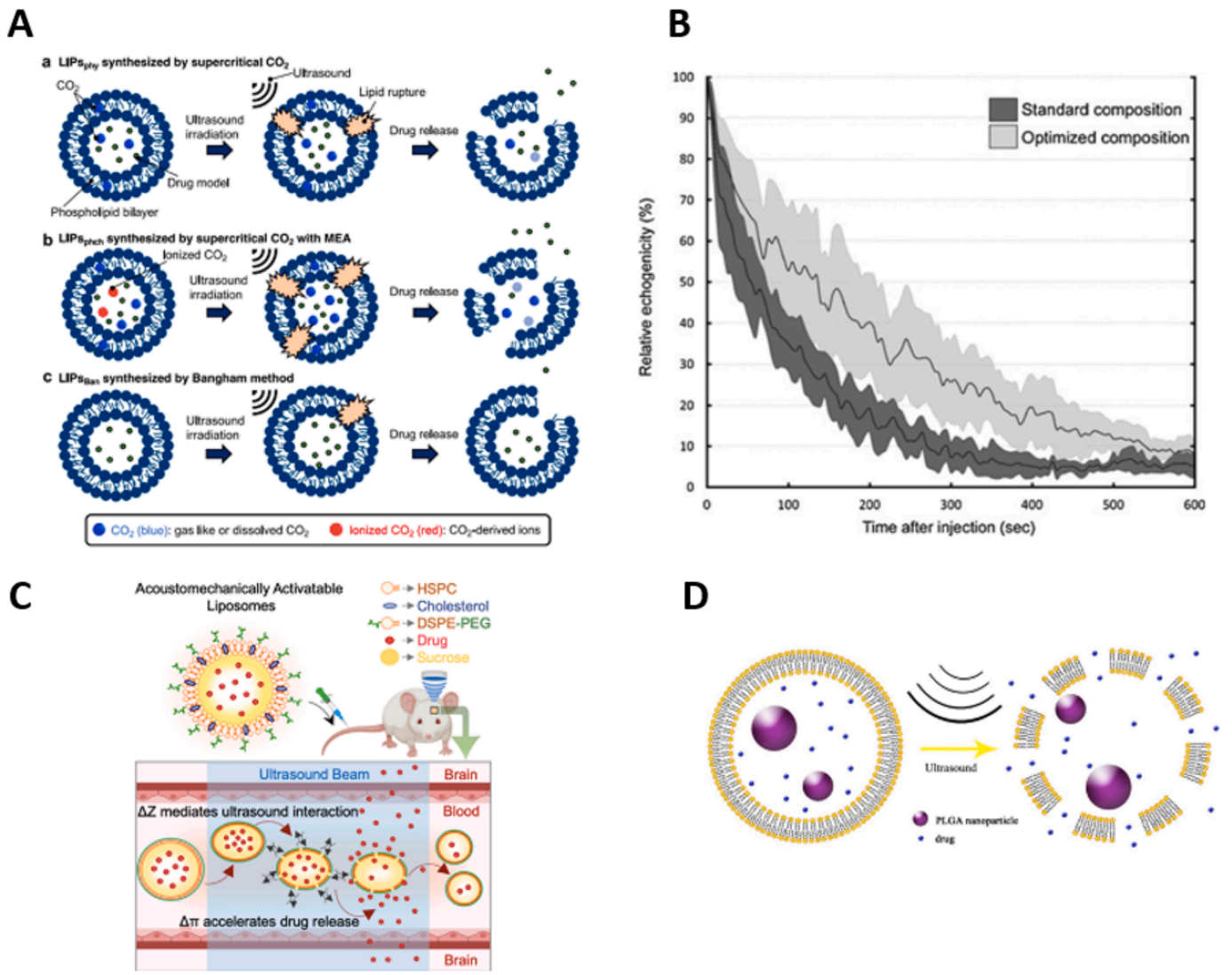

Fig. 9. (A) Schematic representation of the synthesis, US activation and drug release of: (a) echogenic liposomes loaded with dissolved CO_2, (b) echogenic liposomes containing both dissolved CO_2 and ionized CO_2 by adding monoethanolamine during the high pressure CO_2 formulation of liposomes, and (c) conventional liposomes obtained by the Bangham method. From [164]. (B) Kinetics of the relative echogenicity of standard liposomes (i.e., DSPC: DSPE-PEG$_{2000}$ / 94:6) compared to optimized liposomes (i.e., extra coating; DSPC: DSPG: DSPE-PEG2k / 78:10:12). From[165]. (C) Schematic illustration of acoustomechanically activatable liposomes and hypothesised mechanism of action in the bloodstream. From [167]. (D) Illustration of US-triggered release mechanism from PLGA- and drug-loaded acoustic liposomes. From [168].

1 min of US application at 250 MHz (40 and 60 % release, respectively, *versus* 20 % release without sucrose).

4.2.2.3. Liposomes with solid particles loaded in the core. Another interesting strategy to address gas diffusion and leakage from echogenic liposomes has been developed [168] by replacing the gas core with a core containing stable solid nanoparticles. This strategy could also help overcome some limitations for drug delivery applications as the gas core typically does not allow the encapsulation of hydrophilic drugs. Under US exposure, the solid nanoparticles inside the liposomes produce movement leading to the destruction of the surrounding lipid bilayer. Following this approach, liposomes have been formulated using the emulsion solvent evaporation approach to encapsulate both PLGA nanoparticles and the anticancer drug mitoxantrone. Faster drug release from PLGA-loaded liposomes has been observed under physiological conditions (i.e., PBS, pH 7.4) upon US irradiation compared to non-irradiated controls (55.72 % and 8.94 %, after 2 h, respectively). This can be attributed to the vibrations produced by the PLGA nanoparticles that are encapsulated into the liposome's core which leads to membrane disruption and thus faster release (Fig. 9***D***). This innovative approach has also demonstrated higher bioavailability *in vivo* compared to traditional liposomal carriers.

Liposomes are the most widely used technology for designing drug delivery systems due to their biocompatibility, ease of synthesis, and high stability, despite their relatively rapid clearance from the body [161]. In addition, high drug loadings can be achieved with liposomal carriers and their small size (i.e., 100–200 nm) facilitates direct cell uptake. These systems also offer significant advantages for use with acoustic tweezers, as they allow the encapsulation of highly US-sensitive gas in the core, providing strong acoustic contrast for efficient trapping and manipulation with the tweezers. However, it should be noted that the gas core does not allow the encapsulation of hydrophilic drugs and may induce instability due to gas diffusion and leakage. Innovative strategies are currently under investigation to address this issue such as the use of sugar-based liquid cores [167].

4.2.3. Microbubbles

Microbubbles (MBs) are FDA-approved US contrast agents that are

described as gas-filled vesicles (1–10 μm) stabilised by surfactants (i.e., lipids, polymers of proteins)[137]. MBs have been extensively studied for theranostics and drug delivery purposes (Table 4 and Fig. 7) based on the principle of cavitation (i.e., compression and extension of the gaseous core upon exposure to US). They present interesting properties for drug delivery as their surface can be functionalized for active targeting (e.g., antibodies, aptamers) or PEGylated allowing longer residence time in the blood circulation.

One important limitation of MBs is, however, their low drug loading capacity due to the gas core that is unable to incorporate drugs and because of their thin shell that only provides minimal internal space for accommodating substantial amounts of the therapeutic payload. In most cases, drug molecules reside on the outer surface of MBs, either by being electrostatically complexed (i.e., using cationic lipids for complexation with nucleic acids) [169] covalently-coupled [170] or encapsulated within liposomes or NPs that are then coupled to the surface of MBs (Fig. 10***A***) [171]. For instance, to further improve the transfection efficiency of cationic lipoplexes, Lentacker *et al.* have reported the attachment of cationic lipoplexes to MBs using biotin-avidin–biotin linkages. They showed that lipoplexes attached to MBs could transfect cells upon US exposure with a better efficiency than free lipoplexes or pDNA [171]. Furthermore, various gases have been studied for loading MBs as the stability of MBs primarily depends on gas leakage. Air-filled MBs have therefore been studied but often present very short lifetimes in the bloodstream with insufficient amount of stabilizers [172]. By selecting gases that are not soluble in water and in blood (e.g., perfluoropropane [173], perfluorobutane [174], perfluorohexane vapor [175], sulfur hexafluoride [176]), it is possible to increase the lifetime of MBs in the bloodstream.

As previously described in **section 4.2.2**, two types of cavitation are generally described, *stable cavitation* (occurring at lower US intensities) and *inertial cavitation* (occurring at higher US intensities). MBs have been used to enhance cell uptake of various molecules through sonoporation (Fig. 10***B***). This strategy makes use of these cavitation phenomena providing mechanical energy that enables cell membrane permeabilization [177]. This concept has been used to deliver various types of molecules (e.g., nucleic acids [178179] and small molecules [180]) into cells. During *stable cavitation*, the MB's core oscillates in response to the acoustic wave, inducing membrane permeabilization. In contrast, during *inertial cavitation*, pores are typically formed through a jetting shockwave caused by the asymmetrical implosion of the MB [181].

Owing to the implosion and fragmentation of MBs, such cavitation has also been explored to rupture biological barriers and to permeabilize the endothelium of blood vessels [184]. Both *stable and inertial cavitations* were reported to be able to disrupt the blood brain barrier (BBB) which hinders the entry of therapeutics into the brain [185]. One of the first studies reporting BBB opening for drug delivery was the one of Treat and colleagues who could achieve increased doxorubicin concentrations in the brain with Optison, a commercially available bubble-based contrast agent, and the use of focused US [186,187]. Since then, extensive efforts have been made to explore MB cavitation for BBB opening. Nevertheless, MBs' implosion can induce shockwaves that cause damage to the blood vessels, thus cavitation must be better controlled through the optimization of several factors such as the bubble type, acoustic pressure or the animal model [186]. Safe BBB opening generally occurs in a narrow range of pressure (250–500 kPa). For a complete review about BBB opening through MB cavitation, readers are referred to [186].

Despite their limitations, MBs offer key advantages for use with acoustic tweezers and are one of the few particle types that has been already explored with this technology (see **section 5**). These key advantages include high contrast for motion actuation, high versatility for drug delivery, biocompatibility and biodegradability. However, the encapsulation of therapeutic payloads in MBs remains a bottleneck. Besides, their size is rather large (1–10 μm) impeding direct cell uptake. Therefore, acoustic tweezers must be used in combination with inertial or stable cavitation near the target tissue or cells to enable drug delivery from MBs or transfection *via* sonoporation.

4.2.4. Nanodroplets

Nanodroplets (NDs) are sub-microns particles composed of a liquid core surrounded by a surfactant shell[188] (Fig. 7) usually made from biocompatible materials such as lipids (e.g., dipalmitoylphosphatidylcholine (DPPC), distearoyl phosphatidylcholine (DSPC)), proteins (e.g., albumin) or polymers (e.g., PLGA, polycaprolactone (PCL))[189]. Besides their smaller size, their main structural difference with MBs relies on the nature of the particle's core as MBs are constituted by a gas core. The liquid core of NDs is usually formed by liquid perfluorocarbon (PFC) and stabilized by the presence of a surfactant shell. Unlike the gas core of MBs, this liquid part enables easy physical encapsulation of drugs

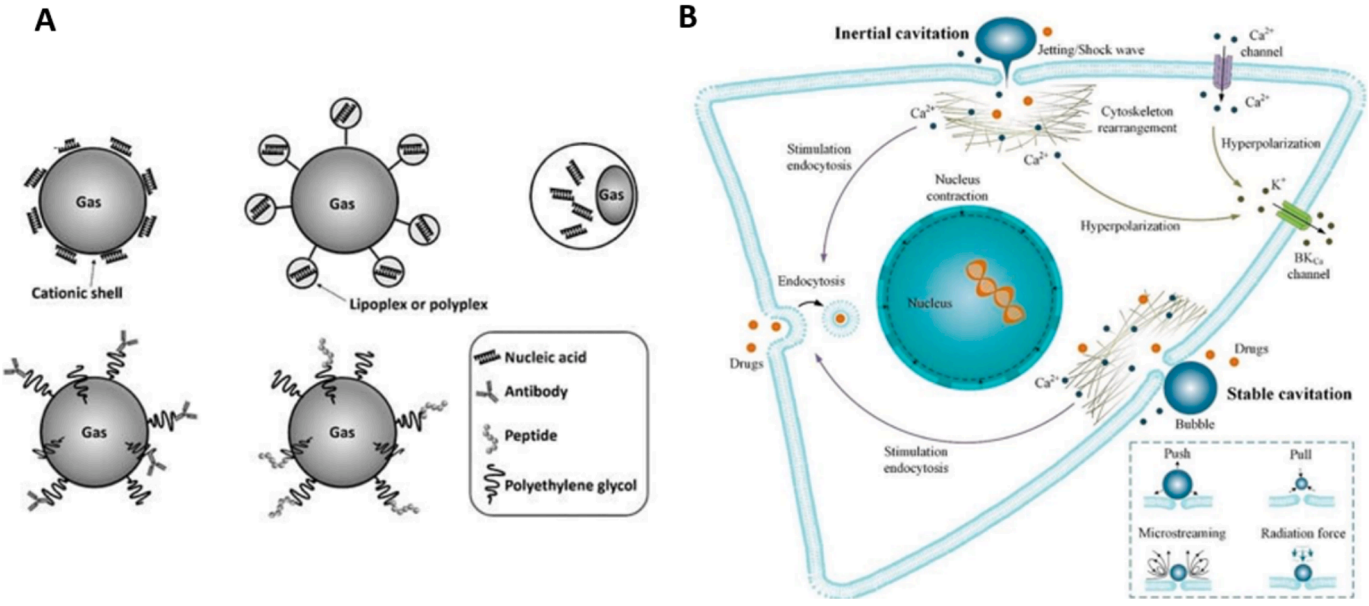

Fig. 10. (A) Schematic representation of MBs' functionalization strategies. (B) sonoporation mechanism for cell penetration of MBs (inertial cavitation). Adapted from [182][183].

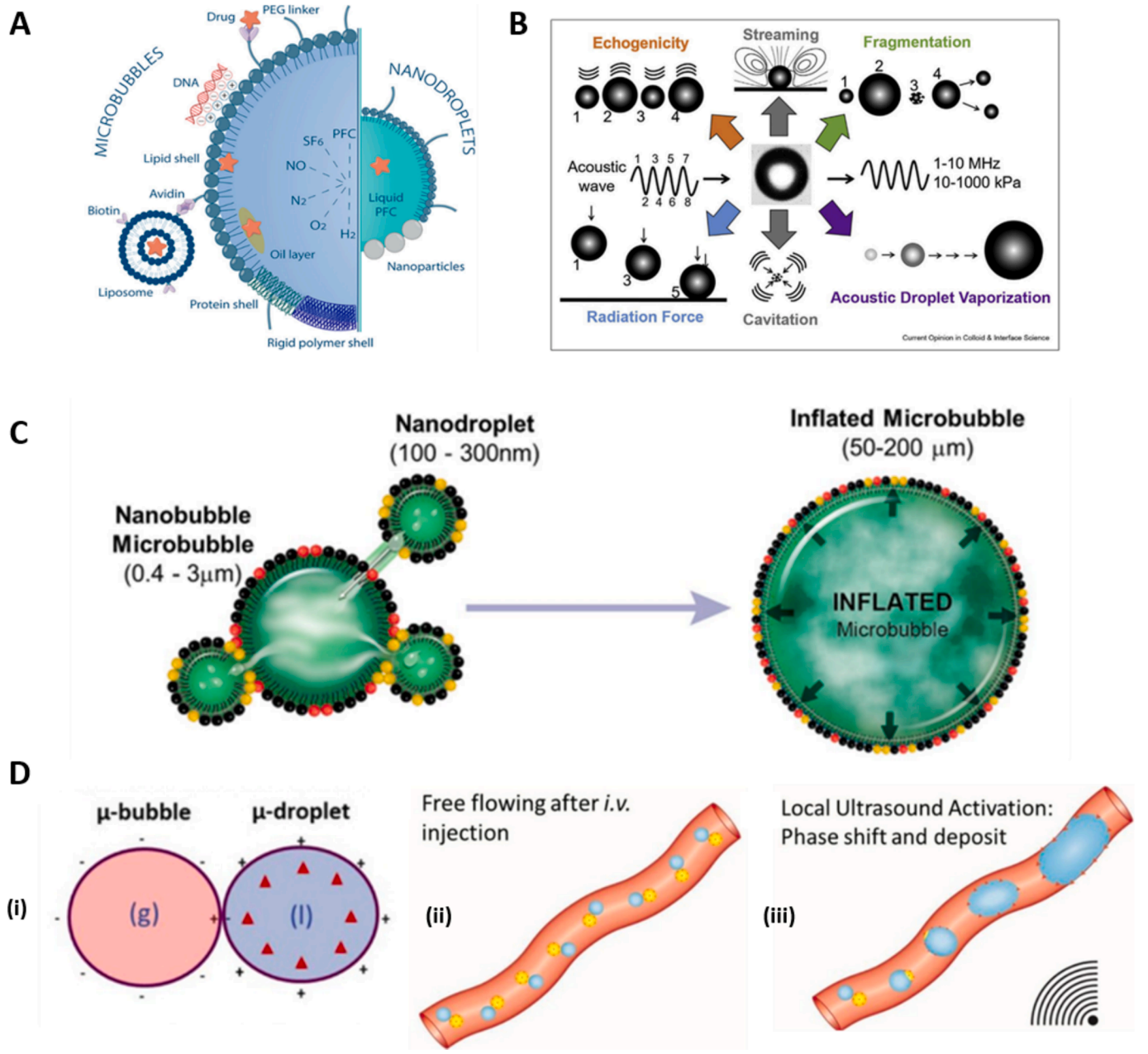

Fig. 11. (A) Schematic comparison of the structure of MBs and NDs. From [188]; (B) Illustration of the different acoustic phenomena observed after acoustic wave irradiation. Adapted from [190]; (C) Representation of microbubble inflation occurring during ADV. From [195]; (D) Schemes of: (i) electrostatic interactions between microbubbles and microdroplets; (ii) intravenous (i.v.) injection of microbubbles and microdroplets leading to the formation of freely flowing clusters in the bloodstream; (iii) phase shift of microdroplets and deposition upon US irradiation leading to enhanced drug delivery. Adapted from [196].

(Table 4 and Fig. 11***A***).

NDs appear as promising carriers for drug delivery due to: (i) their small size (< 1 µm) facilitating cell uptake and (ii) their increased half-life in the bloodstream (i.e., 2–6 h compared to minutes for microbubbles) [189–191] preventing rapid phagocytosis and body clearance. However, NDs in solution have been characterized with poor acoustic contrast, primarily due to their incompressibility [192]. Therefore, several techniques have been developed in order to efficiently vaporize NDs leading to the formation of high-contrast MBs. In this context, acoustic nanodrops have been developed as precursors to MBs which can be vaporized on-demand into bubbles upon exposure to an acoustic field, a process known as *acoustic droplet vaporization* (ADV) (Fig. 11***B***). The ADV technique has been known to enhance acoustic contrast [193] by providing less distortion of the acoustic field and better focus of the acoustic beam in the tissue. These acoustic improvements can induce a higher vascular permeability hence a better targeting efficiency [194]. The smaller size of NDs enhances their ability to extravasate from the leaky vasculature [190], which is characterized by pore sizes ranging from 100 to 1200 nm.

Nonetheless, successful ADV of nanodroplets still requires high acoustic pressure amplitudes for phase-shift and high frequencies due to their small size [190]. Besides, the vaporization mechanism is not clearly understood and controlled. Indeed, the coexistence of liquid perfluorocarbon droplets and gaseous microbubbles in the blood during ADV has been associated to significant side-effects, related to perfluorocarbon transfer from droplets to adjacent microbubbles leading to microbubble inflation [195] (Fig. 11***C***). Nevertheless, the formulation parameters can be tuned in order to better control the bubble inflation

phenomenon. For instance, the nature of the surfactant shell can influence the size of the bubble formed during inflation, as denatured protein-based shells (e.g., bovine serum albumin (BSA)) may physically limit the bubble's growth compared to their lipid counterparts that allow for greater inflation. These improvements can help rescue the US signal without obstructing blood flow thereby improving imaging diagnostic tools as well as increasing the safety of NDs for use in drug delivery applications. The coexistence of nanodroplets and MBs formed during ADV has also inspired the development of innovative treatments such as *acoustic cluster therapy* (ACT) [196]. This approach is based on the administration of negatively-charged MBs and positively-charged microdroplets which can form small clusters of approximately 4 μm through electrostatic interactions (Fig. 11***D (i)***). These freely flowing clusters can be locally activated *in vivo* upon low-frequency US irradiation leading to the phase shift of droplets, local deposition and enhanced delivery (Fig. 11***D (ii)-(iii)***).

The fabrication of NDs can be optimised for drug delivery applications by considering the following factors:

(i) ***the design of the surrounded shell.*** The outer layer can be tailored by changing its chemical composition (e.g., polymer, lipid, proteins, etc.) and by modifying its surface with targeting moieties (e.g. hyaluronic acid, peptides, folic acid (FA)) or stabilising agents (e.g., Tween 20) to improve drug delivery efficiency. For instance, acoustic nanodrops have been synthesised using FA-functionalized PLGA and Fe_3O_4 nanoparticles in the shell, with a core loaded with both perfluoropentane (PFP) and the anticancer drug Dox (Fa-Fe@P-PFP-Dox) (Fig. 12***A***)[197]. FA molecules were grafted to the surface in order to achieve better targeting efficiency for nasopharyngeal carcinoma treatment. The covalent coupling of FA moieties onto the PLGA surface combined with low-intensity focused ultrasound (LIFU) irradiation significantly increased therapeutic activity. Indeed, the cumulative Dox release from FA-conjugated nanodroplets in phosphate buffer saline (PBS) was considerably higher with PFP encapsulation and under LIFU irradiation (Fig. 12***B***), demonstrating that both PFP encapsulation and external US activation are crucial parameters for achieving efficient on-demand Dox release. Furthermore, *in vitro* studies on HNE1 cells demonstrated greater cytotoxicity of FA-based nanodroplets upon LIFU treatment (*Fa-Fe@P-PFP-Dox + LIFU*) compared to droplets without FA decoration (*Fe@P-PFP-Dox + LIFU*) and those without LIFU treatment (*Fa-Fe@P-PFP-Dox*) (Fig. 12***C***). Notably, LIFU treatment alone did not affect cell viability. These FA-functionalized nanodroplets were also associated with higher cellular uptake and tumor accumulation *in vivo*.

The surrounding shell of NDs can also be decorated with solid particles to improve drug payload. Similar to MBs, the use of NDs for drug delivery can be limited by relatively low drug payloads. To address this, azide-liposomes of 120 nm were attached to the dibenzocyclooctyne (DBCO)-functionalized surface of 547 nm nanodroplets *via* "click" chemistry leading to phase changeable droplet-liposome clusters (PDLCs) of 660 nm (Fig. 13***A***) [198]. This conjugation resulted in a 7-fold higher calcein encapsulation compared to azide-blocked DBCO nanodroplets without grafted liposomes. Using ADV, intracellular drug release could be achieved through vascular permeabilization of the vascular endothelium and disruption of the liposomes. After 5 and 10 min of US application at 45 °C, PDLCs demonstrated higher calcein release (35 %) compared to DBCO-blocked droplets and azide liposomes (i.e., no covalent coupling) and to the physical mixture of droplets and liposomes (Fig. 13***B***).

(ii) ***the design of the liquid core.*** The liquid core of NDs allows the encapsulation of various drugs for delivery based on the ADV technique. Their transformation into MBs can then lead to drug release mediated by

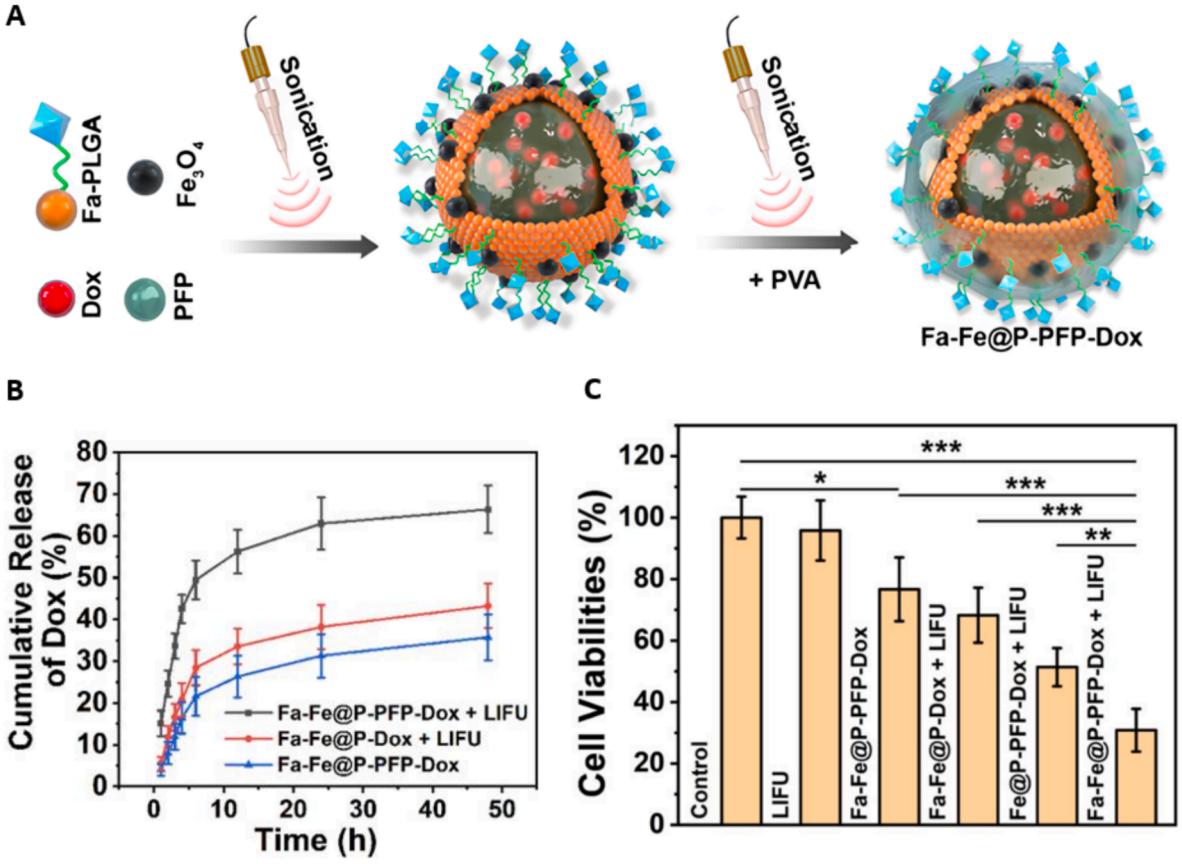

Fig. 12. (A) Schematic illustration of the formulation of NDs decorated with FA-PLGA moieties and a core composed of Dox and PFP gas; (B) Dox release from FA-Fe Dox-loaded NDs with or without LIFU treatment, and with or without a PFP gas core; (C) Relative cell viabilities of HNE1 cells after various treatments. Combined from [197].

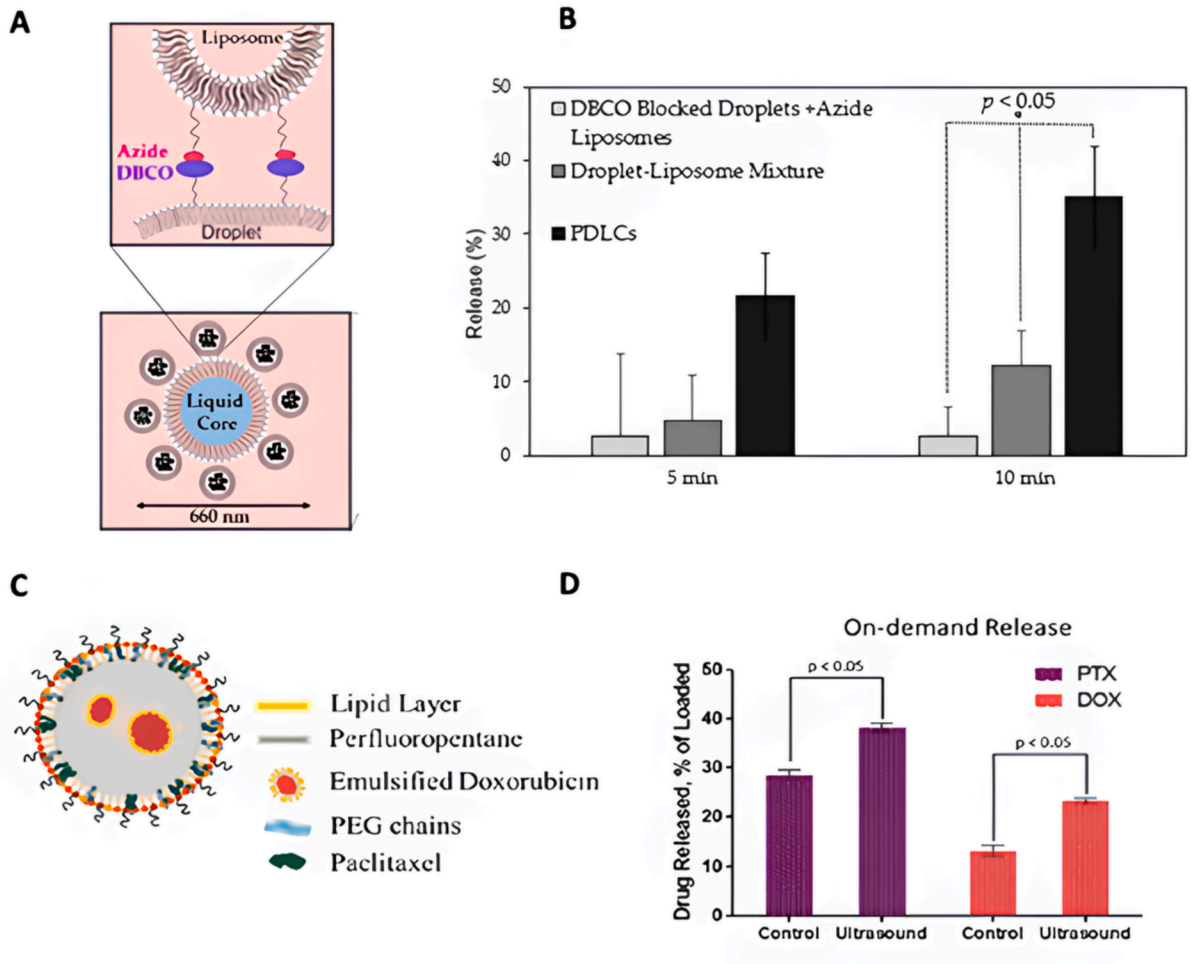

Fig. 13. (A) Schematic illustration of phase-changeable droplet-liposome clusters (PDLCs); (B) Comparison of calcein release upon 5 and 10 min of US irradiation from PDLCs, DBCO-blocked droplets and azide liposomes (i.e., no covalent coupling) and the physical mixture of droplets and liposomes. Combined and ; (C) Schematic representation of perfluoropentane NDs loaded with two anticancer agents (i.e., Ptx and Dox) and surrounded by a lipid shell; (D) Comparison of Ptx and Dox on-demand releases with or without US activation (10 pulses, 1.1 MHz, 10 cycles, 9.6 MPa focal pressure). Combined from adapted from [198][199].

bubble disruption (i.e., US-triggered cavitation). This approach has been developed to provide innovative and on-demand anticancer combination therapy. NDs with a diameter of 332 nm, composed of a perfluoropentane liquid core and a biocompatible lipid shell, were obtained by the double emulsion method [199]. Two anticancer agents, Paclitaxel (Ptx) and Dox, were successfully loaded into the liquid core (Fig. 13***C***) with encapsulation efficiencies of 74.6 % and 60.7 %, respectively. Upon US application (1.1 MHz pulses, 10 cycles, 9.6 MPa focal pressure), the release of both Ptx and and Dox was considerably enhanced compared to control conditions without US (34 and 76 % of increase, respectively), confirming successful droplet vaporization and payload release (Fig. 13***D***). The authors demonstrated *in vitro* and *in vivo* improvements using dual-drug loaded nanodroplets, showing higher cytotoxicity on the triple negative breast cancer cell line MDA-MB-231 compared to single-drug formulations, and a significant delay in tumor growth with US-activated droplets compared to non-activated droplets.

The nature of the liquid composing the core of NDs can also be modified to optimize their acoustic properties. The boiling point of the liquid must be carefully selected as it affects the circulation time in the body and the conditions under which the liquid vaporizes into gas. The most commonly used liquid for designing NDs is hydrophobic perfluorocarbon due to its low partition coefficient which reduces the risk of binding to blood proteins. Different perfluorocarbon molecules have been developed by altering the chain length to achieve varying boiling points. Two perfluorocarbon liquids, decafluorobutane (DFB) and octafluoropropane (OFP), have been used to achieve droplet vaporization [198] at 45 and 37 °C, respectively. The use of OFP compared to DFB has demonstrated more efficient vaporization, attributed to the lower activation threshold of the perfluorocarbon, and higher total calcein release after ADV. Besides, higher concentrations of perfluorocarbon liquid can increase droplet size, which may reduce delivery efficiency by decreasing extravasation efficacy and/or reducing half-life in the bloodstream. Interestingly, perfluorocarbon liquids have also been identified as stabilizing agents for high-ionic liquids in NDs which can be valuable for delivering high-ionic prodrugs [200].

The use of NDs for drug delivery is currently being intensively explored and remains promising thanks to their biocompatibility and high potential for extravasation and tissue penetration. Significant optimization of targeting and delivery efficiencies can be achieved by modifying both the core and shell compositions as well as by modulating the acoustic parameters (e.g. pressure, frequency, number of cycles, pulse mode). Acoustic tweezers have already been employed to manipulate droplets on hydrophobic surfaces [201], but further studies are needed to extend this manipulation to drug delivery, improve the understanding of the *in vivo* biodistribution of nanodroplets and enhance their colloidal stability.

4.2.5. *Antibubbles*

Antibubbles (ABs) derive their name from their structure, which is the opposite of a soap bubble (Fig. 7) [202]. While soap bubbles consist

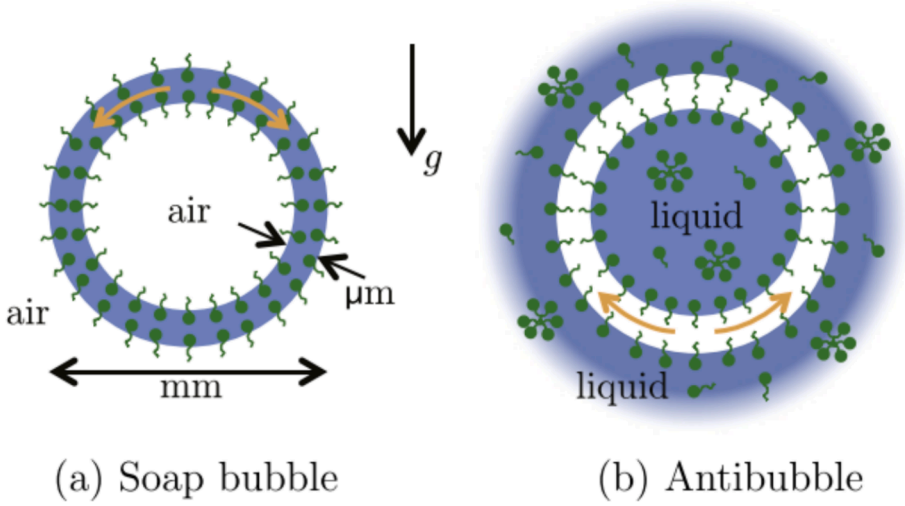

Fig. 14. Schematic representations of a soap bubble (a) and of an antibubble (b). Adapted from [202].

of a thin liquid film surrounding a gaseous core, anti-bubbles consist of a thin gaseous film surrounding a liquid core (Fig. 14). For decades, ABs were not considered for clinical use due to their short lifespan (ranging from seconds to minutes) even with surfactant stabilization [203]. However, efforts have been made to extend their lifetime, and pickering stabilization (i.e. stabilization of an emulsion using solid particles) with silica nanoparticles has resulted in ABs with a lifetime exceeding 10 h [204]. Methods to produce more stable microscale ABs have been described in the literature, with emulsification emerging as the standard method for their preparation [204,205].

Recently, ABs have been investigated for drug delivery purposes (Table 4) as alternatives to MBs, owing to their liquid core, which allows for higher drug encapsulation efficiency compared to MBs, where encapsulation is limited to the shell or achieved by grafting liposomes to their surface [206]. Another reason is their interesting acoustic properties for US-mediated drug delivery, as they exhibit a similar contrast to MBs. At lower acoustic amplitudes, the cavitation of ABs can be precisely controlled and used for imaging, while at higher acoustic amplitudes, they can rupture and release their therapeutic payloads [207]. Studies have shown that ABs exhibit symmetric oscillation at low acoustic amplitudes (200 kPa) and asymmetric oscillation at higher amplitudes (1 MPa), with limited negative excursion due to their incompressible liquid core [208]. Kotopoulis *et al.* evaluated the capacity of ABs to encapsulate calcein for image-guided and US-triggered drug delivery. Antibubbles (size < 10 μm) were stabilized by silica NPs and were able to release calcein using clinical US settings, with stability and detectability comparable to commercially available US contrast agents [206]. Silica NPs provide stability in neutral and acidic environments. The same group also explored calcium carbonate ($CaCO_3$) NPs as stabilizers for ABs encapsulating methylene blue, aiming to induce cargo release in acidic environments (e.g., for gastric drug delivery) [209]. A burst release was achieved in pH 2 buffer (60 % released), while under neutral conditions, 70 % of the cargo remained encapsulated. Multicompartmental ABs have also been developed, enabling the encapsulation of multiple drugs [210].

Acoustic tweezers have not yet been explored for controlling the motion of ABs for drug delivery purposes. However, due to their ample inner space, which facilitates drug encapsulation, and their gaseous layer providing contrast, ABs hold great potential to be acoustically driven by tweezers to target specific tissues. Despite the progress made, further efforts are needed to improve encapsulation efficiency and prolong stability. Besides, only "model" drugs (e.g., calcein, methylene blue) have been investigated so far, leaving a gap in the encapsulation of therapeutically relevant drugs or nucleic acids.

5. Application of acoustic tweezers to drug delivery

Although there are currently few reports in the literature on the use of acoustic tweezers for drug delivery, this section outlines various successful examples investigated *in vitro* or using *ex vivo* or *in vivo* models.

Selective and contactless trapping of objects using acoustic tweezers has emerged as a promising technique for the manipulation of biological objects such as cells, particles and microorganisms.[235] Precise spatial control of drug diffusion is an effective strategy for achieving targeted drug delivery. The safety of US for cells and tissues, when operated below cavitation and deleterious heating thresholds – defined by the mechanical and thermal indexes – is well-documented and demonstrated daily in medical imaging. The key advantages of applying acoustic tweezers for biomedical applications are their (i) high biocompatibility, (ii) ability to operate *in vivo* in opaque media and (iii) capacity to exert large forces (up to μNewtons) [40] with low power (Table 1). Since the radiation force is proportional to the intensity of the beam divided by the wave speed, the significantly lower speed of sound compared to light (by a factor of 10^5) allows the manipulation of particles using acoustic tweezers with much lower power than optical tweezers, resulting in considerably higher safety for patients.

5.1. *In vitro and ex vivo investigations of acoustic tweezers for drug delivery*

The unique capability of acoustic tweezers to manipulate particles in various media makes them highly attractive for guiding DDS to diseased areas. Therefore, it is crucial to first understand the acoustic manipulation processes in different biological media *in situ*.

Huynh *et al.* proposed a modeling study [236] focused on two different media: (i) simulated blood and (ii) a dual-layered fat-muscle model. The densities and speeds of sound in these environments (i.e., blood, fat and muscle) are slightly different (i.e., 1043, 909 and 1060 kg/m^3 and 1570, 1450 and 1585 m/s, respectively) which can affect the formation of acoustic traps and their ability to manipulate particles. Cellulose particles with a diameter of 0.56 mm were used as models to assess the formation of acoustic traps in these simulated media. These particles tend to be attracted to points where the potential energy (i.e. the energy created due to presence of particles into the acoustic field) is the lowest, moving towards the center of the acoustic traps (twin or vortex traps). The morphology and magnitude of acoustic traps were relatively comparable in the fat-muscle two layer-model and the single blood medium. These results are particularly relevant for studies

focusing on particle behavior and acoustic trap formation in various biological media, providing valuable insights for future *in vitro* and *in vivo* research with acoustic tweezers. Other key factors must be considered when using acoustic tweezers for controlled motion of particles *in vitro* and *ex vivo*, such as the driving force (i.e., the acoustic radiation force or the acoustic streaming force), the frictional force (i.e., interactions between particles and biological fluid), and heat conversion (i.e., sound to heat), which could be harmful for tissues [236]. Baresh & Garbin have explored the potential of particle-covered microbubbles (so-called armoured bubbles) for drug delivery. These particle-covered microbubbles are of high interest because (i) they exhibit a strong acoustic contrast, (ii) they carry some micro/nano particles and (iii) they are stable against dissolution [237]. Another *in situ* study [75] focused on the directed payload delivery from microbubbles coated with 500-nm polystyrene particles (PPs) in an agarose-based hydrogel using acoustical vortices. The authors demonstrated that these bubbles could only be trapped laterally (no axial trap). However, axial stabilization was possible by counteracting the Archimedes force with the radiation force. Furthermore, upon US activation, they observed different release patterns of PPs depending on the size of microbubbles over a distance greater than a few bubble diameters: (i) "plumes", (ii) multidirectional and (iii) bidirectional patterns (Fig. 15). These patterns were influenced by the vibrating mode of the acoustically excited bubbles. The "plumes" release pattern was described as a violent ejection of particles, with final speeds 3 to 5 times higher than typical microstreaming flow velocities observed around oscillating bubbles.

Ex vivo studies have been conducted using holographic acoustic tweezers to manipulate nanocarrier clusters of 100 nm [238]. The biocompatibility of these nanoclusters was confirmed in two different mouse cells lines, 4 T1 (breast cancer) and NIH3T3 (fibroblasts), showing high cell viability of up to 90 % with increasing particle concentration up to 200 μg/mL. The authors also demonstrated successful 3D manipulation and rotation of nanoclusters on porcine ribs with a thickness of 30 mm (Fig. 16***A-B***) using a multielement system composed of 30 ultrasound transducers (UTs) with single-side arrangement. They showed that rapid trapping of the particles could be achieved at the trapping point. Interestingly, the temperature at the focal point only slightly increased (from 24.4 to 27.6 °C over 15 min), further confirming the safe use of this type of tweezers for bioapplications. However, this *ex vivo* model lacks real flow conditions. Moreover, the distance between the tweezers and the targeted area in this model was 75 mm, which remains too short for application in the human body. Nevertheless, this study paves the way for directed drug delivery through the simple manipulation and accumulation of particles to a desired site.

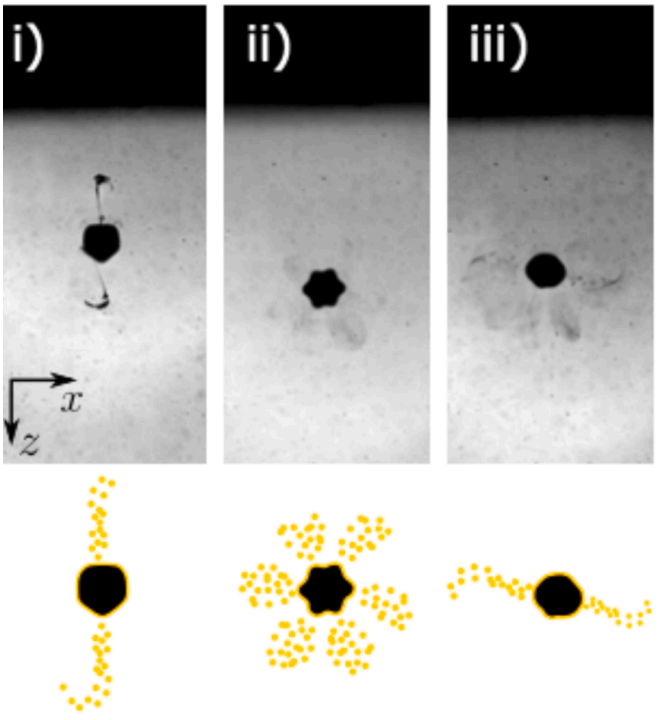

Fig. 15. Release images and patterns from microbubbles coated with PS beads: (i) "plumes", (i) multidirectional and (iii) bidirectional. Adapted from [75].

Acoustic vortex beams have also been explored for transdermal drug delivery. The transdermal route offers a more convenient administration method, allowing for self-administration and reducing the pain associated with injection. A study by Li *et al.*, reported on a transdermal transmission system developed in a water bath at 37 °C, consisting of a donor chamber filled with physiological saline solution and a receptor chamber containing the drug solution [239]. These two chambers were separated by a cellulose membrane, which mimicked the porous structure and mechanical strength of the transdermal barrier (Fig. 16***C***). A focused acoustic beam with a maximum acoustic pressure of 200 kPa enhanced the permeability of the cellulose membrane to glycerin (50 %) and hyaluronic acid (0.9 %) by enlarging its pores through the application of a transverse acoustic radiation force at the piconewton level.

An acoustic patch has also been designed for efficient transdermal drug delivery [74]. It was developed using a piezoelectric transducer and acoustic metamaterials that can be loaded with drug molecules (Fig. 17***A***). These acoustic metamaterials generate localised acoustic streaming to transport therapeutics from the porous human epidermis to deeper tissues. This model was tested in an *ex vivo* model using fresh mouse skin tissues to evaluate stratum corneum penetration and control of the drug release. The patch was loaded with Rhodamine B as a model drug, and the release was investigated after the application of acoustic waves for 3 min at a power density of 2.4 W/cm^2. Fluorescent imaging analysis of mouse skin sections revealed a maximum penetration depth of 500 μm and a dye diffusion depth of 1000 μm. The acoustic patch also demonstrated the ability to control drug release over specific time periods under multi-burst stimulation by tuning the acoustic power density (Fig. 17***B-C***). These results are promising for *in vivo* application of the patch, particularly regarding the achieved penetration depth and dye diffusion, aiming for controlled and targeted drug release.

5.2. *In vivo investigations of acoustic tweezers for drug delivery*

The use of acoustic tweezers for *in vivo* applications has not yet been widely explored, as several challenges still need to be addressed, including achieving high tissue penetration, ensuring biocompatibility and safety, developing adaptable animal setups, and generating a strong trapping force [240]. Moreover, applying acoustics to *in vivo* tissues must overcome the issue of tissue aberration, i.e. acoustic wave distortion caused by tissue heterogeneities. The transdermal acoustic patch, previously mentioned in **section 5.1**, was also tested *in vivo* on C57BL/6 mice [74]. The delivery efficiency of Rhodamine B was compared among 4 groups (Fig. 18): (i) transdermal patch with acoustic treatment (+); (ii) transdermal patch without acoustic treatment, corresponding to passive diffusion (−); (iii) subcutaneous (SC) injection and (iv) blank. Using In Vivo Imaging Systems (IVIS), the authors managed to demonstrate that mice treated with the acoustic patch (+) exhibited a larger diffused area of the dye (i.e., higher photon intensity) and longer dye retention time (Fig. 18***A***) within the skin compared to the other three groups. Biodistribution studies revealed that mice treated with acoustics (+) retained larger amounts of dye in muscle tissue than the other groups (Fig. 18***A-B***). This may be explained by increased dye diffusion and uptake due to acoustic waves into the blood vessels of the SC tissue, leading to higher amounts of dye diffusing towards muscle tissues. This acoustic patch represents a promising example of an acoustic-driven DDS, providing more efficient delivery than SC administration and passive diffusion strategies.

Strong flow conditions within the bloodstream represent an

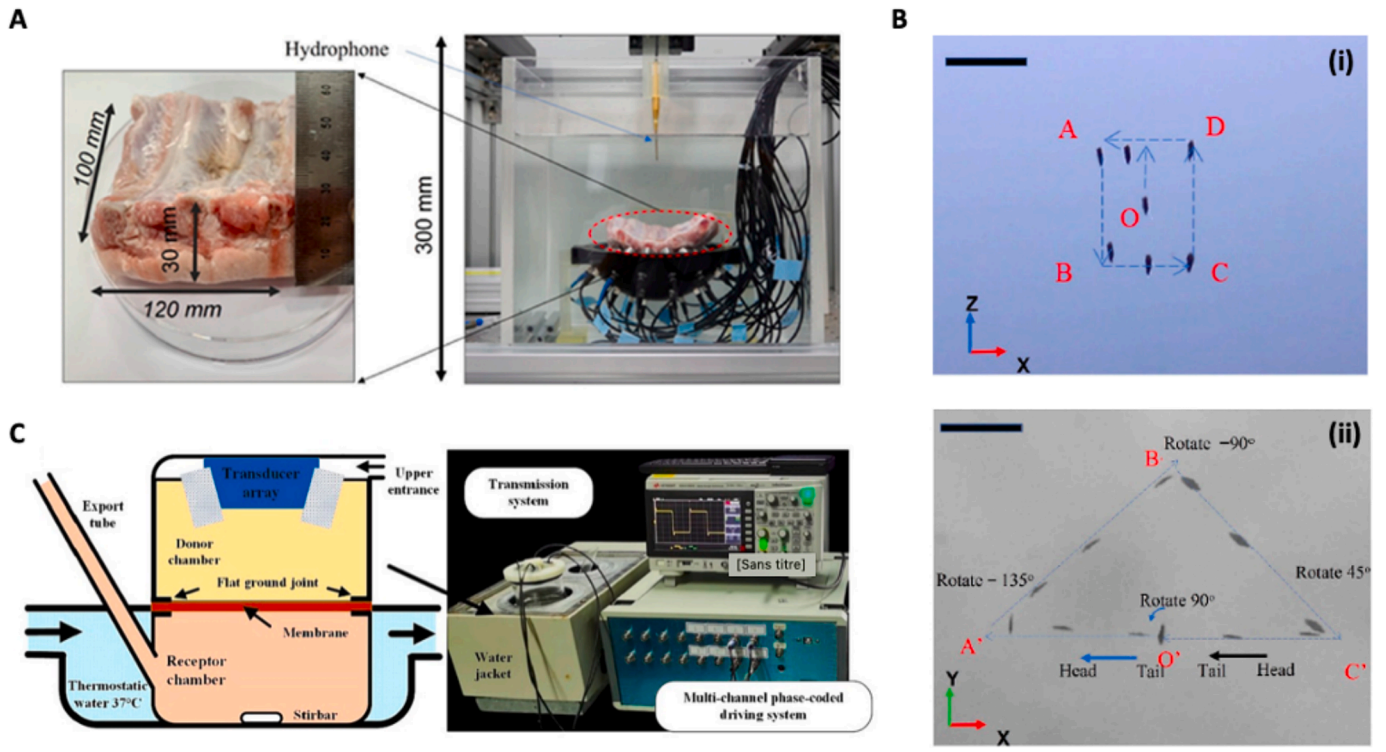

Fig. 16. (A) Ex vivo porcine rib dimensions and experimental set-up, including the acoustic tweezers; (B) Time-lapse of manipulation in the XOY plane (i) and rotation in the XOZ plane (ii). Scale bar: 2 mm. Adapted from [238]; (C) Schematic of the transdermal transmission system, composed of two different chambers separated by a cellulose membrane (left) and photograph of the transmission system (right). Adapted from [239].

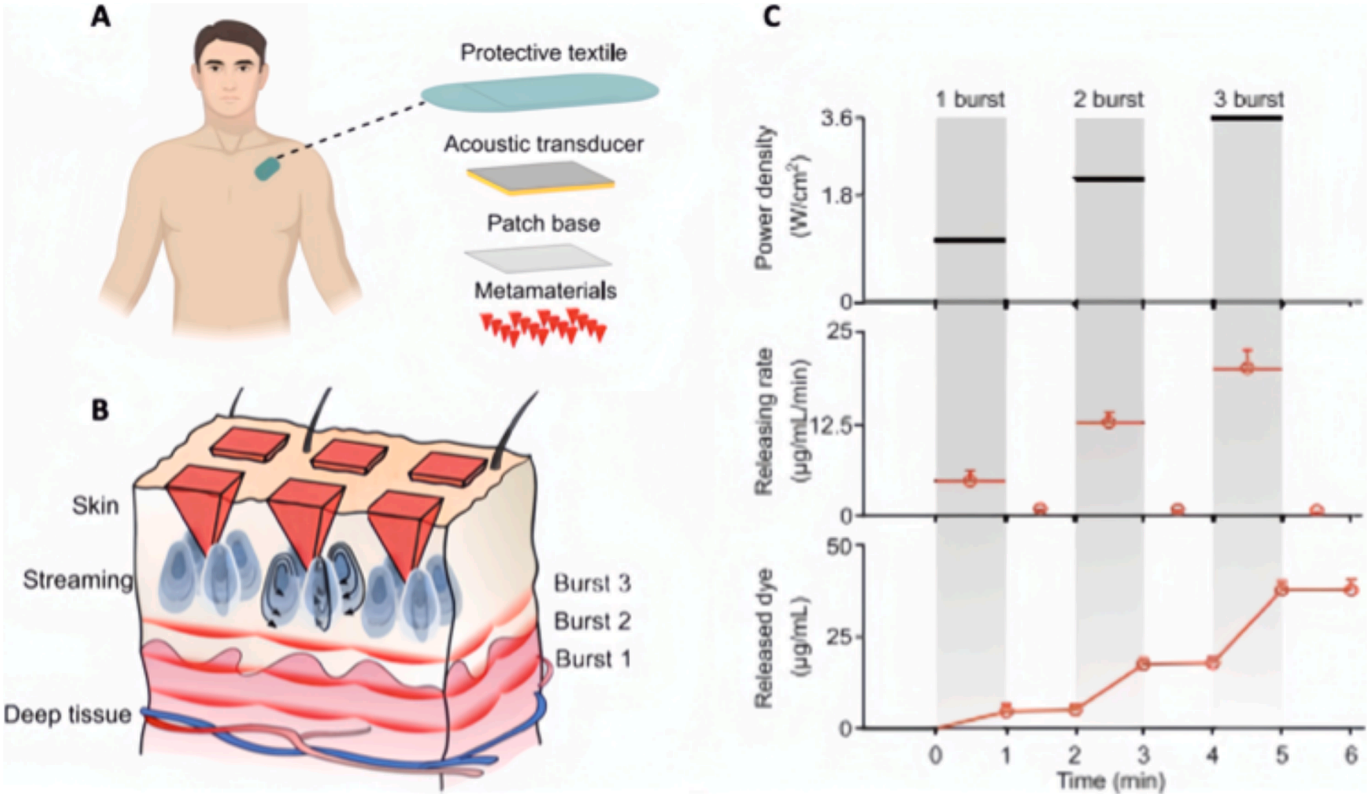

Fig. 17. (A) Schematic illustration of the transdermal patch for application on the human body; (B) Schematic of the multi-burst stimulation and its effect on skin; (C) Evolution of power density and controlled release rate and amount of Rhodamine B during 3 bursts. Adapted from [74].

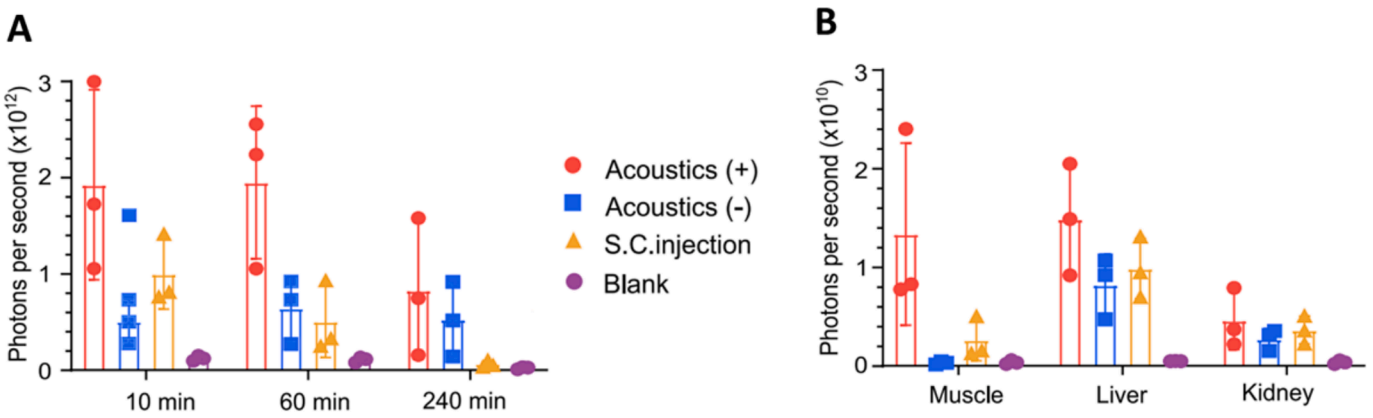

Fig. 18. In vivo biodistribution studies comparing acoustic-driven transdermal drug delivery, SC injection and passive diffusion. (A) Quantification of Rhodamine B dye release over time for the 4 different groups (mean ± s.e.m., n = 3 mice per group, independent experiments). (B) Quantification of Rhodamine B dye in mouse muscle, liver, and kidney 24 h after the indicated treatments (mean ± s.e.m., n = 3 mice per group, independent experiments). From [74].

important obstacle to the successful implementation of acoustic tweezers in living organisms. In this context, DDS must have a strong acoustic contrast compared to the surrounding biological fluid to generate sufficient trapping force driving them towards the US beam axis. Therefore, studying the use of acoustic tweezers to trap and manipulate particles in the blood circulation is of great interest for future drug delivery applications. Tornado-inspired acoustic vortex tweezers have been developed to trap and manipulate lipid-based microbubbles in the blood circulation *in vivo* [240]. These tweezers have been designed to enable non-invasive intravascular trapping of particles by generating a potential well, allowing the use of relatively low-frequency ultrasound (3 MHz) (Fig. 19***A***). Trapping performance was studied in mice using a skin-fold dorsal window chamber model (Fig. 19***B***). The authors successfully demonstrated the trapping of microbubbles without disrupting blood flow and no occlusions of small vessels was observed, paving the way for *in vivo* delivery of microbubbles through the bloodstream (Fig. 19***C***). Key acoustic parameters for acoustic trapping under flow conditions *in vivo* were identified: (i) *the pressure*, which should not be exceeded to avoid MB collapse and (ii) *the frequency*, which could be lowered to enhance penetration. However, it is important to note that this *in vivo* study did not simulate pathological conditions such as diabetes or ischemia, which could significantly alter the acoustic properties of the targeted region and potentially affect the efficacy of acoustic vortex tweezers.

The feasibility of trapping of particles in blood vessels has also been tested using single-beam acoustic tweezers and curved surfaces with a thickness of 0.8 mm to mimic blood vessels [241]. These acoustic

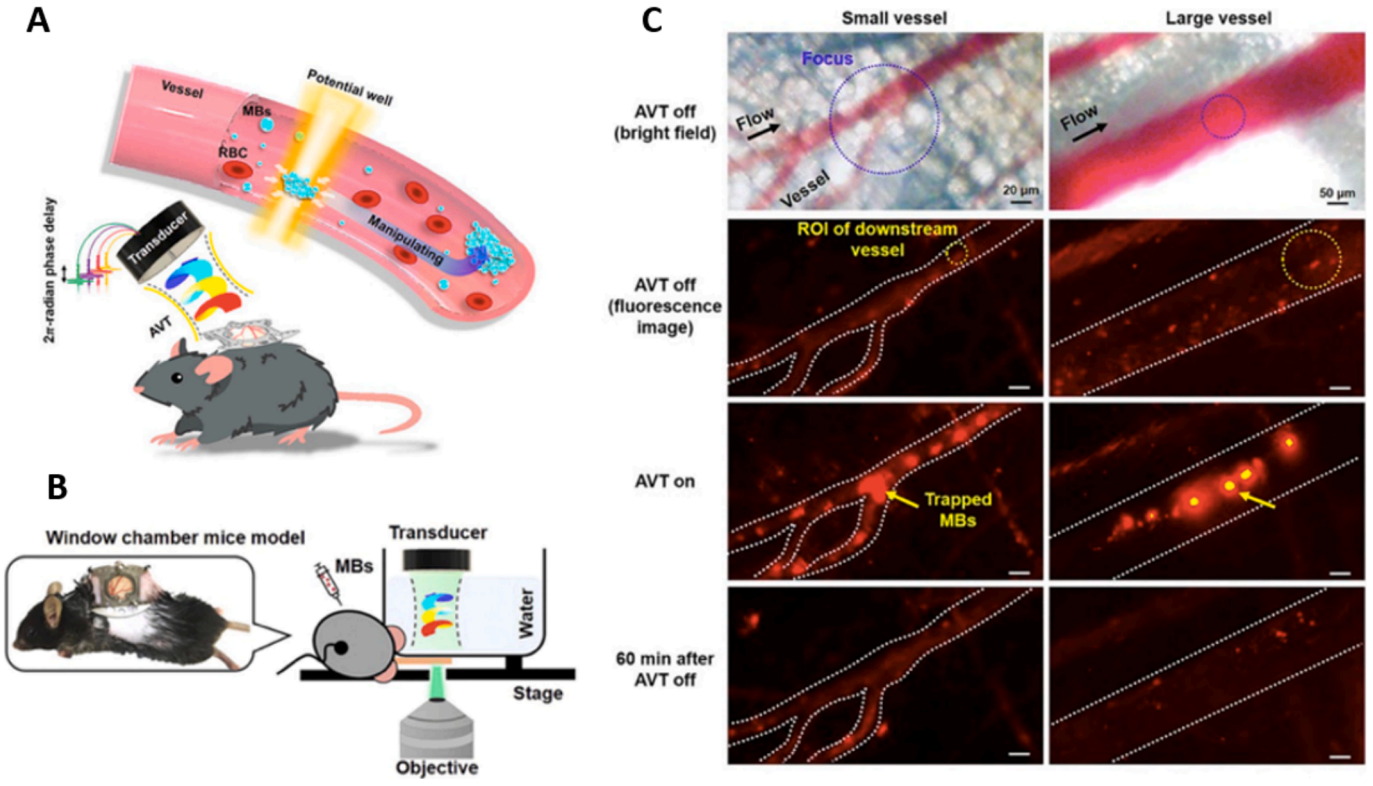

Fig. 19. (A) Schematic representation of the generation of a potential well by tornado-inspired acoustic vortex tweezers for enhanced trapping and manipulation of microbubbles in the bloodstream *in vivo*. (B) Illustration of the experimental set-up consisting of a window chamber mice model and the acoustic platform. (C) In vivo fluorescence images of small and large vessels (20 and 200 μm in diameter, respectively) acquired before, during, and after application of tornado-inspired acoustic tweezers. From [240].

tweezers have been able to manipulate microparticles in this model, confirming the potential translation of acoustic tweezers for *in vivo* applications in small animals, such as rats and mice. Additionally, vortex beams have been used to trap and move particles *in vivo* in pigs (Fig. 20) [37]. Glass spheres with a 3 mm diameter were successfully guided through three preprogrammed paths within the urinary bladders of live pigs using a vortex beam power of 10 W. This beam was able to penetrate body wall thicknesses ranging from 18 to 31 mm. After US irradiation, each pig was evaluated for tissue safety and no injury was observed along the bladder wall.

These examples are highly promising for the use of acoustic tweezers in the field of drug delivery, particularly regarding their ability to trap and guide particles, which could significantly enhance targeting efficiency *in vivo*. However, the biological application of acoustic tweezers for improving drug delivery efficiency remains highly challenging. Key considerations include the biocompatibility and safety of acoustic tweezers, as well as the design of the experimental setup and the dynamic flow conditions in living organisms, which could greatly impact their efficacy.

6. Conclusions and perspectives

In this review, we have highlighted the assets of acoustic tweezers for drug delivery through theoretical insights and practical examples. Firstly, acoustic tweezers enable the manipulation of a wide range of biocompatible and biodegradable materials. Secondly, acoustic manipulation can be effectively performed deep within tissues, with strong trapping forces reaching up to microNewtons.

6.1. Challenges for use of acoustic tweezers in drug delivery

Nevertheless, several challenges (Fig. 21) must be addressed before acoustic tweezers can be clinically implemented for *in vivo* drug delivery:

(i) the *acoustic field* must be carefully engineered to trap the targeted drug carriers in complex environments, including dynamic flow conditions, while ensuring their directed transport to target sites. In this respect, laterally focused or 3D-focused beams are of primary interest.

(ii) the *appropriate wavefield synthesis technology* must be selected to combine precision with operational simplicity. Emerging holographic techniques may help address these challenges.

(iii) *careful selection of drug carriers* is crucial; they must exhibit biocompatibility, demonstrate effective drug release capabilities, and possess sufficient acoustic contrast to be manipulated by ultrasound forces. To this aim, they must fulfil specific criteria. First, their *size* must allow mobility in biological fluids. Larger systems might induce obstructions in small-caliber blood vessels and also result in limited cellular uptake. For this purpose, **liposomes** and **nanodroplets** appear as the most interesting systems due to their size of a few hundred nanometers and ease of formulation. Second, the drug carriers must have sufficient *contrast* (i.e., density and/or compressibility) to be used with acoustic tweezers. For this, **microbubbles** and **antibubbles** are promising due to their intrinsically low density and high compressibility despite their larger size. Finally, the DDS must allow for *sufficient encapsulation* of the agent to be delivered. While microbubbles show great promise due to their clinical approval as imaging agents, their strong acoustic contrast and their active exploration in ultrasound-

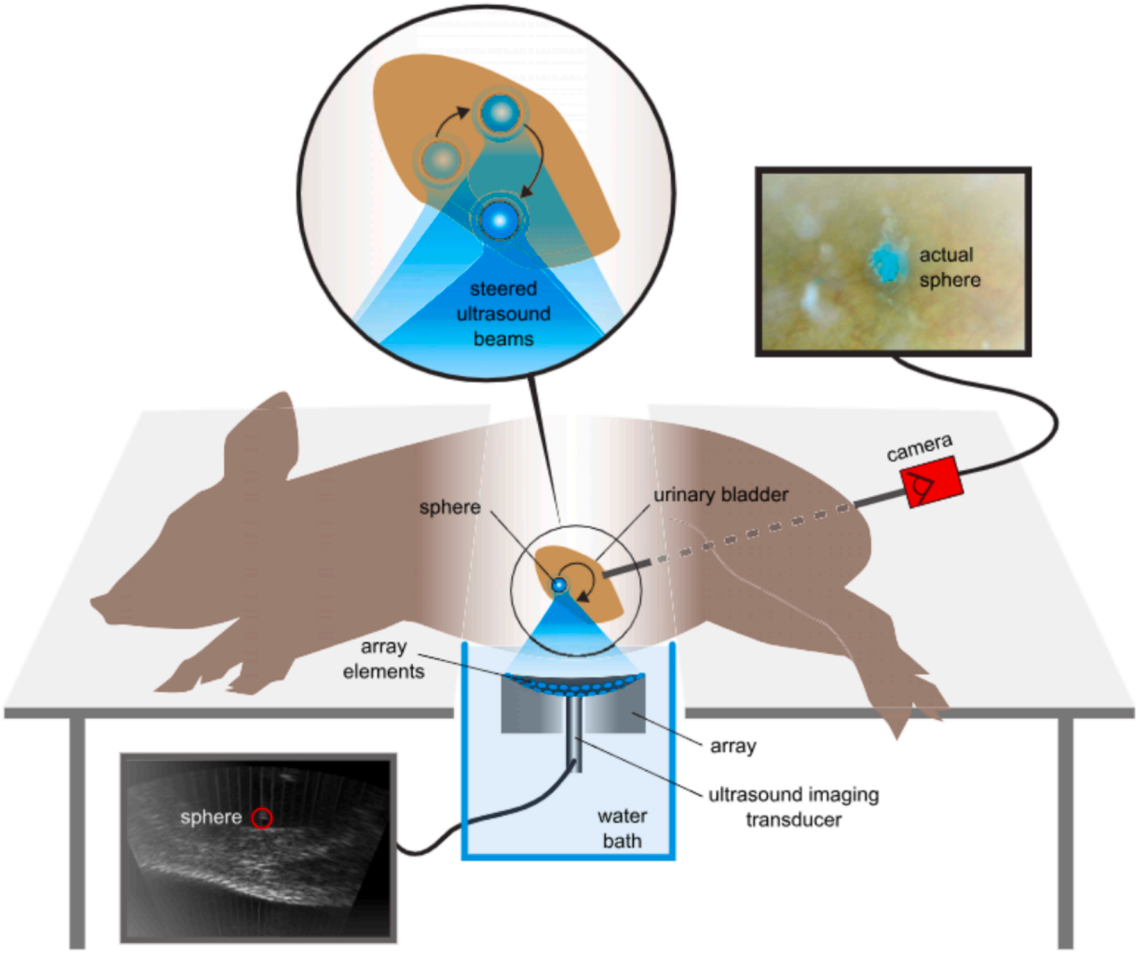

Fig. 20. Schematic representation of the experimental set-up allowing the acoustic manipulation of 3 mm- glass spheres in the urinary bladder of live pigs. From [37].

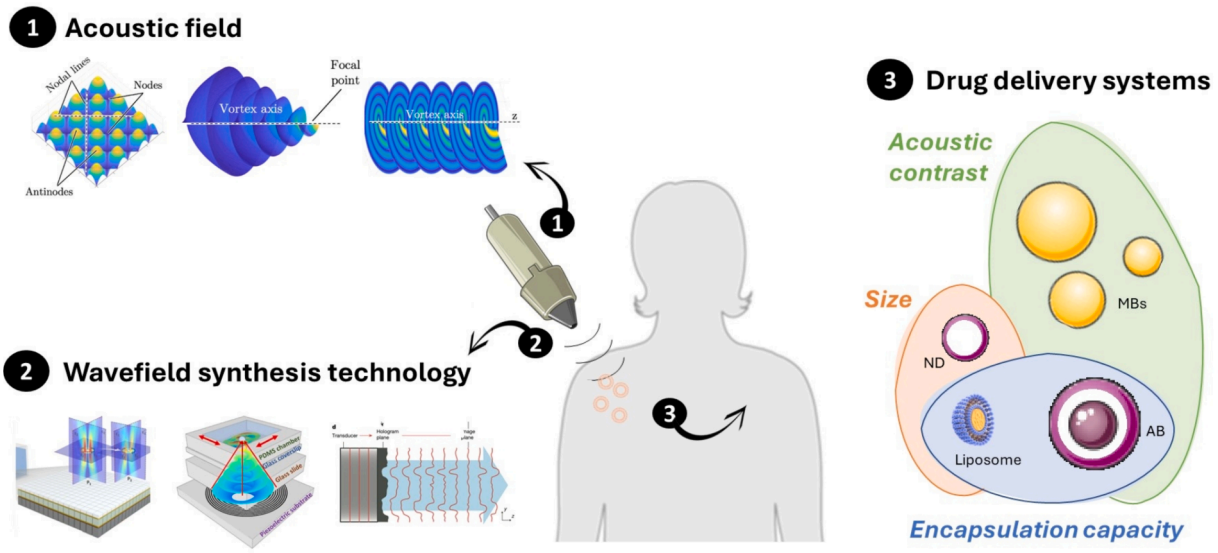

Fig. 21. Schematic guidelines for the design of acoustic tweezers and drug carriers for improved targeted drug delivery (ND: nanodroplet, AB: antibubble, MBs: microbubbles).

triggered drug delivery, their gaseous core limits their ability to encapsulate high drug loads. **Antibubbles** and **liposomes**, which contain a liquid core, may address this encapsulation limitation.

6.2. Clinical considerations

The design of new drug delivery systems has to address clinical challenges [242] and to overcome major limitations, including but not limited to: (i) dose-related issues (e.g., amount, frequency), (ii) pharmacokinetic profiles, (iii) drug side-effects (e.g., local irritation, infections, burst release), (iv) patient compliance (e.g., confort, pain, self-administration, hospital stays).

The use of acoustic tweezers to deliver drugs could solve dose-related problems by improving targeting efficiency and the amount of drug delivered during an injection. By reducing the potential number of drug injections, the use of this new non-invasive technology could help reduce adverse effects and improve patient compliance. Finally, it is essential to remember that acoustic tweezers operate at frequencies and amplitudes that are within the clinical range of ultrasound, which minimises the risk of adverse effects in tissues. As demonstrated in the last part of this review, acoustic tweezers have the potential to work effectively *in vivo* for particle manipulation and targeted drug delivery. However, other *in vitro* and *in vivo* studies are required, as well as a more advanced exploration of the fundamentals of acoustic tweezer technologies to enable easier and faster clinical translation. This highlights the crucial need for interdisciplinary teamwork to develop this innovative technology which has the potential to revolutionise the field of drug delivery.

Declaration of Generative AI and AI-assisted technologies in the writing process.

During the preparation of this work the author(s) used chatGPT4 in order to improve language and readability. After using this tool/service, the author(s) reviewed and edited the content as needed and take(s) full responsibility for the content of the publication.

Acknowledgments

This work is supported by the ERC grant (DYE-LIGHT, 10107587) obtained by F.S, and the IUF Grant, the ERC Generator, and International Chair Will funded by Université de Lille and obtained by M.B.

Conflicts of interest

Michael Baudoin has 4 unlicenced patents on acoustic tweezers.

Data availability

No data was used for the research described in the article.

References

[1] Recent advances in prodrug-based nanoparticle therapeutics, Eur. J. Pharm. Biopharm. 165 (2021) 219–243.
[2] J.M. Harris, N.E. Martin, M. Modi, Pegylation, Clin. Pharmacokinet. 40 (2012) 539–551.
[3] B. Pelaz, C. Alexiou, R.A. Alvarez-Puebla, F. Alves, A.M. Andrews, S. Ashraf, L. P. Balogh, L. Ballerini, A. Bestetti, C. Brendel, S. Bosi, M. Carril, W.C.W. Chan, C. Chen, X. Chen, X. Chen, Z. Cheng, D. Cui, J. Du, C. Dullin, A. Escudero, N. Feliu, M. Gao, M. George, Y. Gogotsi, A. Grünweller, Z. Gu, N.J. Halas, N. Hampp, R.K. Hartmann, M.C. Hersam, P. Hunziker, J. Jian, X. Jiang, P. Jungebluth, P. Kadhiresan, K. Kataoka, A. Khademhosseini, J. Kopeček, N. A. Kotov, H.F. Krug, D.S. Lee, C.-M. Lehr, K.W. Leong, X.-J. Liang, M.L. Lim, L. M. Liz-Marzán, X. Ma, P. Macchiarini, H. Meng, H. Möhwald, P. Mulvaney, A. E. Nel, S. Nie, P. Nordlander, T. Okano, J. Oliveira, T.H. Park, R.M. Penner, M. Prato, V. Puntes, V.M. Rotello, A. Samarakoon, R.E. Schaak, Y. Shen, S. Sjöqvist, A.G. Skirtach, M.G. Soliman, M.M. Stevens, H.-W. Sung, B.Z. Tang, R. Tietze, B.N. Udugama, J. Scott VanEpps, T. Weil, P.S. Weiss, I. Willner, Y. Wu, L. Yang, Z. Yue, Q. Zhang, Q. Zhang, X.-E. Zhang, Y. Zhao, X. Zhou, W.J. Parak, D. Applications, of,, Nanomedicine (2017), https://doi.org/10.1021/acsnano.6b06040.
[4] Microparticles produced by the hydrogel template method for sustained drug delivery, Int. J. Pharm. 461 (2014) 258–269.
[5] Poly(ethylene glycol) methacrylate hydrolyzable microspheres for transient vascular embolization, Acta Biomater. 10 (2014) 1194–1205.
[6] Recent advances in the development of microparticles for pulmonary administration, Drug Discov. Today 25 (2020) 1865–1872.
[7] M.T. Manzari, Y. Shamay, H. Kiguchi, N. Rosen, M. Scaltriti, D.A. Heller, Targeted drug delivery strategies for precision medicines, Nat Rev Mater 6 (2021) 351–370.
[8] K. Braeckmans, K. Buyens, W. Bouquet, C. Vervaet, P. Joye, F. De Vos, L. Plawinski, L. Doeuvre, E. Angles-Cano, N.N. Sanders, J. Demeester, S.C. De Smedt, Sizing nanomatter in biological fluids by fluorescence single particle tracking, Nano Lett. 10 (2010) 4435–4442.
[9] A. Ashkin, J.M. Dziedzic, J.E. Bjorkholm, S. Chu, Observation of a single-beam gradient force optical trap for dielectric particles, Opt. Lett. 11 (1986) 288.
[10] K.C. Neuman, S.M. Block, Optical trapping, Rev. Sci. Instrum. 75 (2004) 2787–2809.
[11] S. Chu, L. Hollberg, J.E. Bjorkholm, A. Cable, A. Ashkin, Three-dimensional viscous confinement and cooling of atoms by resonance radiation pressure, Phys. Rev. Lett. 55 (1985) 48–51.
[12] E.L. Raab, M. Prentiss, A. Cable, S. Chu, D.E. Pritchard, Trapping of neutral sodium atoms with radiation pressure, Phys. Rev. Lett. 59 (1987) 2631–2634.

[13] N. Schlosser, G. Reymond, I. Protsenko, P. Grangier, Sub-poissonian loading of single atoms in a microscopic dipole trap, Nature 411 (2001) 1024–1027.
[14] M. Karski, L. Förster, J.-M. Choi, A. Steffen, W. Alt, D. Meschede, A. Widera, Quantum walk in position space with single optically trapped atoms, Science 325 (2009) 174–177.
[15] H. Kim, W. Lee, H.-G. Lee, H. Jo, Y. Song, J. Ahn, In situ single-atom array synthesis using dynamic holographic optical tweezers, Nat. Commun. 7 (2016) 1–8.
[16] Optical tweezers in single-molecule biophysics, Nature Reviews Methods Primers 1 (2021) 1–1.
[17] M.D. Wang, H. Yin, R. Landick, J. Gelles, S.M. Block, Stretching DNA with optical tweezers, Biophys. J. 72 (1997) 1335–1346.
[18] A. Ashkin, J.M. Dziedzic, Optical trapping and manipulation of viruses and bacteria, Science 235 (1987) 1517–1520.
[19] H. Zhang, K.-K. Liu, Optical tweezers for single cells, J. R. Soc. Interface (2008), https://doi.org/10.1098/rsif.2008.0052.
[20] K.C. Neuman, E.H. Chadd, G.F. Liou, K. Bergman, S.M. Block, Characterization of photodamage to Escherichia coli in optical traps, Biophys. J. 77 (1999) 2856–2863.
[21] Y. Liu, D.K. Cheng, G.J. Sonek, M.W. Berns, C.F. Chapman, B.J. Tromberg, Evidence for localized cell heating induced by infrared optical tweezers, Biophys. J. 68 (1995) 2137–2144.
[22] Y. Liu, G.J. Sonek, M.W. Berns, B.J. Tromberg, Physiological monitoring of optically trapped cells: assessing the effects of confinement by 1064-nm laser tweezers using microfluorometry, Biophys. J. 71 (1996) 2158–2167.
[23] A. Blázquez-Castro, Optical Tweezers: Phototoxicity and Thermal Stress in Cells and Biomolecules, Micromachines (Basel) 10 (2019), https://doi.org/10.3390/mi10080507.
[24] S. Corsetti, K. Dholakia, Optical manipulation: advances for biophotonics in the 21st century, JBO 26 (2021) 070602.
[25] X. Li, J.F. Lovell, J. Yoon, X. Chen, Clinical development and potential of photothermal and photodynamic therapies for cancer, Nat. Rev. Clin. Oncol. 17 (2020) 657–674.
[26] P.S. Kollipara, X. Li, J. Li, Z. Chen, H. Ding, Y. Kim, S. Huang, Z. Qin, Y. Zheng, Hypothermal opto-thermophoretic tweezers, Nat. Commun. 14 (2023) 1–9.
[27] L. Lin, X. Peng, X. Wei, Z. Mao, C. Xie, Y. Zheng, Thermophoretic Tweezers for Low-Power and Versatile Manipulation of Biological, Cells (2017), https://doi.org/10.1021/acsnano.7b00207.
[28] R. Piazza, A. Parola, Thermophoresis in colloidal suspensions, J. Phys. Condens. Matter 20 (2008) 153102.
[29] E.L. Talbot, J. Kotar, L. Parolini, L. Di Michele, P. Cicuta, Thermophoretic migration of vesicles depends on mean temperature and head group chemistry, Nat. Commun. 8 (2017) 15351.
[30] A. Kotnala, Y. Zheng, Opto-thermophoretic fiber tweezers, Nanophotonics 8 (2019) 475–485.
[31] Med. Laser Appl 25 (2010) 84–92.
[32] F. D'Agata, F.A. Ruffinatti, S. Boschi, I. Stura, I. Rainero, O. Abollino, R. Cavalli, C. Guiot, Magnetic Nanoparticles in the Central Nervous System: Targeting Principles, Applications and Safety Issues, Molecules 23 (2017) 9.
[33] A. Farzin, S.A. Etesami, J. Quint, A. Memic, A. Tamayol, Magnetic Nanoparticles in Cancer Therapy and Diagnosis, Adv. Healthc. Mater. 9 (2020) 1901058.
[34] J.F. Liu, B. Jang, D. Issadore, A. Tsourkas, Use of magnetic fields and nanoparticles to trigger drug release and improve tumor targeting, Wiley Interdiscip. Rev. Nanomed. Nanobiotechnol. 11 (2019) e1571.
[35] E.K. Schneider-Futschik, F. Reyes-Ortega, Advantages and Disadvantages of Using Magnetic Nanoparticles for the Treatment of Complicated Ocular Disorders, Pharmaceutics 13 (2021) 1157.
[36] M. Baudoin, J.-L. Thomas, Acoustic Tweezers for Particle and Fluid Micromanipulation, Annu. Rev. Fluid Mech. 52 (2020) 205–234.
[37] M.A. Ghanem, A.D. Maxwell, Y.-N. Wang, B.W. Cunitz, V.A. Khokhlova, O. A. Sapozhnikov, M.R. Bailey, Noninvasive acoustic manipulation of objects in a living body, Proc. Natl. Acad. Sci. U. S. A. 117 (2020) 16848–16855.
[38] R.A. Sahely, J.-C. Gerbedoen, N. Smagin, R. Chutani, O.B. Matar, M. Baudoin, Ultra-high frequency vortex-based tweezers for microparticles manipulation with high spatial selectivity and nanoNewton forces (2022), https://doi.org/10.48550/ARXIV.2203.05214.
[39] H. Wu, Z. Tang, R. You, S. Pan, W. Liu, H. Zhang, T. Li, Y. Yang, C. Sun, W. Pang, X. Duan, Manipulations of micro/nanoparticles using gigahertz acoustic streaming tweezers, Nanotechnol. Precis. Eng. 5 (2022) 023001.
[40] D. Baresch, J.-L. Thomas, R. Marchiano, Observation of a Single-Beam Gradient Force Acoustical Trap for Elastic Particles: Acoustical Tweezers, Phys. Rev. Lett. 116 (2016) 024301.
[41] M. Baudoin, J.-C. Gerbedoen, A. Riaud, O.B. Matar, N. Smagin, J.-L. Thomas, Folding a focalized acoustical vortex on a flat holographic transducer: Miniaturized selective acoustical tweezers, Sci Adv 5 (2019) eaav1967.
[42] M. Baudoin, J.-L. Thomas, R.A. Sahely, J.-C. Gerbedoen, Z. Gong, A. Sivery, O. B. Matar, N. Smagin, P. Favreau, A. Vlandas, Spatially selective manipulation of cells with single-beam acoustical tweezers, Nat. Commun. 11 (2020) 4244.
[43] M.E. Mcintyre, On the "wave momentum" myth, J. Fluid Mech. 106 (1981) 331.
[44] P.B. Muller, R. Barnkob, M.J.H. Jensen, H. Bruus, A numerical study of microparticle acoustophoresis driven by acoustic radiation forces and streaming-induced drag forces, Lab Chip 12 (2012) 4617–4627.
[45] W. Qiu, H. Bruus, P. Augustsson, Particle-size-dependent acoustophoretic motion and depletion of micro- and nano-particles at long timescales, Phys. Rev. E 102 (2020) 013108.
[46] O.A. Sapozhnikov, M.R. Bailey, Radiation force of an arbitrary acoustic beam on an elastic sphere in a fluid, J. Acoust. Soc. Am. 133 (2013) 661–676.
[47] M. Settnes, H. Bruus, Forces acting on a small particle in an acoustical field in a viscous fluid, Phys. Rev. E 85 (2012) 016327.
[48] A. Ozcelik, R. Becker, T.J. Huang, Acoustic Technologies in Biology and Medicine, John Wiley & Sons, 2023.
[49] Q. Wang, A. Riaud, J. Zhou, Z. Gong, M. Baudoin, Acoustic Radiation Force on Small Spheres Due to Transient Acoustic Fields, Phys. Rev. Appl. 15 (2021) 044034.
[50] G.T. Silva, H. Bruus, Acoustic interaction forces between small particles in an ideal fluid, Phys. Rev. E 90 (2014) 063007.
[51] E.B. Lima, J.P. Leão-Neto, A.S. Marques, G.C. Silva, J.H. Lopes, G.T. Silva, Nonlinear Interaction of Acoustic Waves with a Spheroidal Particle: Radiation Force and Torque Effects, Phys. Rev. Appl. 13 (2020) 064048.
[52] G.T. Silva, An expression for the radiation force exerted by an acoustic beam with arbitrary wavefront (L), J. Acoust. Soc. Am. 130 (2011) 3541–3544.
[53] D. Baresch, J.-L. Thomas, R. Marchiano, Three-dimensional acoustic radiation force on an arbitrarily located elastic sphere, J. Acoust. Soc. Am. 133 (2013) 25–36.
[54] Z. Gong, M. Baudoin, Equivalence between angular spectrum-based and multipole expansion-based formulas of the acoustic radiation force and torque, J. Acoust. Soc. Am. 149 (2021) 3469.
[55] Z. Gong, M. Baudoin, Single Beam Acoustical Tweezers Based on Focused Beams: A Numerical Analysis of Two-Dimensional and Three-Dimensional Trapping Capabilities, Phys. Rev. Appl. 18 (2022) 044033.
[56] P.B. Muller, M. Rossi, Á.G. Marín, R. Barnkob, P. Augustsson, T. Laurell, C. J. Kähler, H. Bruus, Ultrasound-induced acoustophoretic motion of microparticles in three dimensions, Phys. Rev. E 88 (2013) 023006.
[57] N. Nama, P.-H. Huang, T.J. Huang, F. Costanzo, Investigation of acoustic streaming patterns around oscillating sharp edges, Lab Chip 14 (2014) 2824–2836.
[58] S. Cleve, M. Guédra, C. Mauger, C. Inserra, P. Blanc-Benon, Microstreaming induced by acoustically trapped, non-spherically oscillating microbubbles, J. Fluid Mech. 875 (2019) 597–621.
[59] J.W. Strutt, I. On the circulation of air observed in Kundt's tubes, and on some allied acoustical problems, Philosophical Transactions of the Royal Society of London (1884). DOI: 10.1098/rstl.1884.0002.
[60] W.L. Nyborg, Acoustic Streaming near a Boundary, J. Acoust. Soc. Am. 30 (1958) 329–339.
[61] M.F. Hamilton, Y.A. Ilinskii, E.A. Zabolotskaya, Acoustic streaming generated by standing waves in two-dimensional channels of arbitrary width, J. Acoust. Soc. Am. 113 (2003) 153–160.
[62] M.F. Hamilton, Y.A. Ilinskii, E.A. Zabolotskaya, Thermal effects on acoustic streaming in standing waves, J. Acoust. Soc. Am. 114 (2003) 3092–3101.
[63] P.B. Muller, H. Bruus, Numerical study of thermoviscous effects in ultrasound-induced acoustic streaming in microchannels, Phys. Rev. E 90 (2014) 043016.
[64] P.B. Muller, H. Bruus, Theoretical study of time-dependent, ultrasound-induced acoustic streaming in microchannels, Phys. Rev. E 92 (2015) 063018.
[65] I. Reyt, V. Daru, H. Bailliet, S. Moreau, J.-C. Valière, D. Baltean-Carlès, C. Weisman, Fast acoustic streaming in standing waves: generation of an additional outer streaming cell, J. Acoust. Soc. Am. 134 (2013) 1791–1801.
[66] V. Daru, I. Reyt, H. Bailliet, C. Weisman, D. Baltean-Carlès, Acoustic and streaming velocity components in a resonant waveguide at high acoustic levels, J. Acoust. Soc. Am. 141 (2017) 563–574.
[67] J.T. Karlsen, W. Qiu, P. Augustsson, H. Bruus, Acoustic Streaming and Its Suppression in Inhomogeneous Fluids, Phys. Rev. Lett. 120 (2018) 054501.
[68] W.L. Nyborg, Acoustic Streaming due to Attenuated Plane Waves, J. Acoust. Soc. Am. 25 (1953) 68–75.
[69] C.P. Lee, T.G. Wang, Near-boundary streaming around a small sphere due to two orthogonal standing waves, J. Acoust. Soc. Am. 85 (1989) 1081–1088.
[70] A.Y. Rednikov, S.S. Sadhal, Acoustic/steady streaming from a motionless boundary and related phenomena: generalized treatment of the inner streaming and examples, J. Fluid Mech. 667 (2011) 426–462.
[71] J. Lei, P. Glynne-Jones, M. Hill, Acoustic streaming in the transducer plane in ultrasonic particle manipulation devices, Lab Chip 13 (2013) 2133–2143.
[72] J. Lei, M. Hill, P. Glynne-Jones, Numerical simulation of 3D boundary-driven acoustic streaming in microfluidic devices, Lab Chip 14 (2013) 532–541.
[73] J.S. Bach, H. Bruus, Theory of pressure acoustics with viscous boundary layers and streaming in curved elastic cavities, J. Acoust. Soc. Am. 144 (2018) 766–784.
[74] J. Xu, H. Cai, Z. Wu, X. Li, C. Tian, Z. Ao, V.C. Niu, X. Xiao, L. Jiang, M. Khodoun, M. Rothenberg, K. Mackie, J. Chen, L.P. Lee, F. Guo, Acoustic metamaterials-driven transdermal drug delivery for rapid and on-demand management of acute disease, Nat. Commun. 14 (2023) 869.
[75] D. Baresch, V. Garbin, Acoustic trapping of microbubbles in complex environments and controlled payload release, Proc. Natl. Acad. Sci. U. S. A. 117 (2020) 15490–15496.
[76] V. Dvořák, Ueber die Entstehungsweise der Kundt'schen Staubfiguren, Ann. Phys. 227 (1874) 634–639.
[77] C. Eckart, Vortices and Streams Caused by Sound Waves, Phys. Rev. 73 (1948) 68.
[78] A. Riaud, M. Baudoin, O. Bou Matar, J.-L. Thomas, P. Brunet, On the influence of viscosity and caustics on acoustic streaming in sessile droplets: an experimental and a numerical study with a cost-effective method, J. Fluid Mech. 821 (2017) 384–420.
[79] V. Gusev, O. Rudenko, Nonsteady quasi-one-dimensional acoustic streaming in unbounded volumes with hydrodynamic non-linearity, Sog. Phys. Acoust. 25 (1979) 493–497.

[80] B. Moudjed, V. Botton, D. Henry, H. Ben Hadid, J.-P. Garandet, Scaling and dimensional analysis of acoustic streaming jets, Phys. Fluids 26 (2014) 093602.
[81] J. Orosco, J. Friend, Modeling fast acoustic streaming: Steady-state and transient flow solutions, Phys. Rev. E 106 (2022) 045101.
[82] O. Dubrovski, J. Friend, O. Manor, Theory of acoustic streaming for arbitrary Reynolds number flow, J. Fluid Mech. 975 (2023) A4.
[83] V. Daru, B. Vincent, M. Baudoin, High-speed and acceleration micrometric jets induced by GHz streaming: A numerical study with direct numerical simulations, J. Acoust. Soc. Am. 155 (2024) 2470–2481.
[84] B. Moudjed, V. Botton, D. Henry, S. Millet, J.P. Garandet, H., Ben Hadid, Near-field acoustic streaming jet, Phys. Rev. E 91 (2015) 033011.
[85] Phys. Procedia 70 (2015) 151–154.
[86] A. Riaud, M. Baudoin, J.-L. Thomas, O.B. Matar, Cyclones and attractive streaming generated by acoustical vortices, Phys. Rev. E 90 (2014) 013008.
[87] Z. Hong, J. Zhang, B.W. Drinkwater, Observation of Orbital Angular Momentum Transfer from Bessel-Shaped Acoustic Vortices to Diphasic Liquid-Microparticle Mixtures, Phys. Rev. Lett. 114 (2015) 214301.
[88] Y. Fan, J. Zhang, B. Wei, B.W. Drinkwater, Controllable patterns and streaming of plane acoustic vortex with annular piezoelectric arrays excitation, Phys. Fluids 33 (2021) 032009.
[89] S. Song, J. Zhou, A. Marcianò, A. Riaud, Contactless generation and trapping of hydrodynamic knots in sessile droplets by acoustic screw dislocations, Phys. Fluids 34 (2022) 064101.
[90] X. Guo, Z. Ma, R. Goyal, M. Jeong, W. Pang, P. Fischer, X. Duan, T. Qiu, Acoustofluidic Tweezers for the 3D Manipulation of Microparticles, in: in: 2020 IEEE International Conference on Robotics and Automation (ICRA), 2020, https://doi.org/10.1109/icra40945.2020.9197265.
[91] S.J. Raymond, D.J. Collins, R. O'Rorke, M. Tayebi, Y. Ai, J. Williams, A deep learning approach for designed diffraction-based acoustic patterning in microchannels, Sci Rep 10 (2020) 8745.
[92] D.J. Collins, C. Devendran, Z. Ma, J.W. Ng, A. Neild, Y. Ai, Acoustic tweezers via sub-time-of-flight regime surface acoustic waves, Sci Adv 2 (2016) e1600089.
[93] A. Haake, J. Dual, Contactless micromanipulation of small particles by an ultrasound field excited by a vibrating body, J. Acoust. Soc. Am. 117 (2005) 2752–2760.
[94] S. Oberti, A. Neild, J. Dual, Manipulation of micrometer sized particles within a micromachined fluidic device to form two-dimensional patterns using ultrasound, J. Acoust. Soc. Am. 121 (2007) 778–785.
[95] S. Oberti, A. Neild, R. Quach, J. Dual, The use of acoustic radiation forces to position particles within fluid droplets, Ultrasonics 49 (2009) 47–52.
[96] J. Shi, D. Ahmed, X. Mao, S.-C.-S. Lin, A. Lawit, T.J. Huang, Acoustic tweezers: patterning cells and microparticles using standing surface acoustic waves (SSAW), Lab Chip 9 (2009) 2890–2895.
[97] B. Hammarström, M. Evander, H. Barbeau, M. Bruzelius, J. Larsson, T. Laurell, J. Nilsson, Non-contact acoustic cell trapping in disposable glass capillaries, Lab Chip 10 (2010) 2251–2257.
[98] G.P. Gautam, Manipulation of Particles and Fluid Using Bulk Acoustic Waves in Microfluidics, 2019.
[99] X. Ding, J. Shi, S.-C.-S. Lin, S. Yazdi, B. Kiraly, T.J. Huang, Tunable patterning of microparticles and cells using standing surface acoustic waves, Lab Chip 12 (2012) 2491–2497.
[100] D.J. Collins, B. Morahan, J. Garcia-Bustos, C. Doerig, M. Plebanski, A. Neild, Two-dimensional single-cell patterning with one cell per well driven by surface acoustic waves, Nat. Commun. 6 (2015) 8686.
[101] T. Laurell, F. Petersson, A. Nilsson, Chip integrated strategies for acoustic separation and manipulation of cells and particles, Chem. Soc. Rev. 36 (2007) 492–506.
[102] †. Filip Petersson, ‡. Lena Åberg, ‡. And Ann-Margret Swärd-Nilsson, †. Thomas Laurell*, Free Flow Acoustophoresis: Microfluidic-Based Mode of Particle and Cell Separation, (2007). DOI: 10.1021/ac070444e.
[103] A. Lenshof, T. Laurell, Continuous separation of cells and particles in microfluidic systems, Chem. Soc. Rev. 39 (2010) 1203–1217.
[104] J. Shi, H. Huang, Z. Stratton, Y. Huang, T.J. Huang, Continuous particle separation in a microfluidic channel via standing surface acoustic waves (SSAW), Lab Chip 9 (2009) 3354–3359.
[105] K. Wang, W. Zhou, Z. Lin, F. Cai, F. Li, J. Wu, L. Meng, L. Niu, H. Zheng, Sorting of tumour cells in a microfluidic device by multi-stage surface acoustic waves, Sens. Actuators B Chem. 258 (2018) 1174–1183.
[106] L. Ren, S. Yang, P. Zhang, Z. Qu, Z. Mao, P.-H. Huang, Y. Chen, M. Wu, L. Wang, P. Li, T.J. Huang, Standing Surface Acoustic Wave (SSAW)-Based Fluorescence-Activated Cell Sorter, Small 14 (2018) e1801996.
[107] S.B.Q. Tran, P. Marmottant, P. Thibault, Fast acoustic tweezers for the two-dimensional manipulation of individual particles in microfluidic channels, Appl. Phys. Lett. 101 (2012) 114103.
[108] X. Ding, S.-C.-S. Lin, B. Kiraly, H. Yue, S. Li, I.-K. Chiang, J. Shi, S.J. Benkovic, T. J. Huang, On-chip manipulation of single microparticles, cells, and organisms using surface acoustic waves, Proceedings of the National Academy of Sciences 109 (2012) 11105–11109.
[109] F. Guo, Z. Mao, Y. Chen, Z. Xie, J.P. Lata, P. Li, L. Ren, J. Liu, J. Yang, M. Dao, S. Suresh, T.J. Huang, Three-dimensional manipulation of single cells using surface acoustic waves, Proceedings of the National Academy of Sciences 113 (2016) 1522–1527.
[110] J. Wu, Acoustical tweezers, J. Acoust. Soc. Am. 89 (1991) 2140–2143.
[111] J. Lee, S.-Y. Teh, A. Lee, H.H. Kim, C. Lee, K.K. Shung, Single beam acoustic trapping, Appl. Phys. Lett. 95 (2009) 073701.
[112] D. Baresch, J.-L. Thomas, R. Marchiano, Spherical vortex beams of high radial degree for enhanced single-beam tweezers, J. Appl. Phys. 113 (2013) 184901.
[113] A. Marzo, S.A. Seah, B.W. Drinkwater, D.R. Sahoo, B. Long, S. Subramanian, Holographic acoustic elements for manipulation of levitated objects, Nat. Commun. 6 (2015) 8661.
[114] Z. Gong, M. Baudoin, Three-Dimensional Trapping and Dynamic Axial Manipulation with Frequency-Tuned Spiraling Acoustical Tweezers: A Theoretical Study, Phys. Rev. Appl. 16 (2021) 024034.
[115] S. Chen, J. Zhou, A. Riaud, Implementation of two-dimensional selective acoustic tweezers merely using four straight interdigitated transducers:a numerical proof of concept of radiation field synthesis by pulsed acoustic waves, (2024). DOI: 10.48550/ARXIV.2406.19523.
[116] Z. Gong, S. Li, Z. Ma, Single focused-beam acoustical tweezers: Trapping cells in 3-D, J. Acoust. Soc. Am. 154 (2023) A263–A.
[117] A. Babazadeh Khameneh, H.R. Chabok, H. Nejat Pishkenari, Optimized integrated design of a high-frequency medical ultrasound transducer with genetic algorithm, SN Applied Sciences 3 (2021) 1–12.
[118] Q. Hu, T. Ma, Q. Zhang, J. Wang, Y. Yang, F. Cai, H. Zheng, 3-D Acoustic Tweezers Using a 2-D Matrix Array With Time-Multiplexed Traps, IEEE Trans. Ultrason. Ferroelectr. Freq. Control 68 (2021) 3646–3653.
[119] K. Melde, A.G. Mark, T. Qiu, P. Fischer, Holograms for acoustics, Nature 537 (2016) 518–522.
[120] K.-Y. Hashimoto, Surface Acoustic Wave Devices in Telecommunications, Springer Berlin Heidelberg, n.d.
[121] J.-L. Thomas, R. Marchiano, Pseudo Angular Momentum and Topological Charge Conservation for Nonlinear Acoustical Vortices, Phys. Rev. Lett. 91 (2003) 244302.
[122] C.R.P. Courtney, C.E.M. Demore, H. Wu, A. Grinenko, P.D. Wilcox, S. Cochran, B. W. Drinkwater, Independent trapping and manipulation of microparticles using dexterous acoustic tweezers, Appl. Phys. Lett. 104 (2014) 154103.
[123] A. Riaud, J.-L. Thomas, E. Charron, A. Bussonnière, O.B. Matar, M. Baudoin, Anisotropic Swirling Surface Acoustic Waves from Inverse Filtering for On-Chip Generation of Acoustic Vortices, Phys. Rev. Appl. 4 (2015) 034004.
[124] A. Riaud, J.-L. Thomas, M. Baudoin, O.B. Matar, Taming the degeneration of Bessel beams at an anisotropic-isotropic interface: Toward three-dimensional control of confined vortical waves, Phys. Rev. E 92 (2015) 063201.
[125] A. Marzo, B.W. Drinkwater, Holographic acoustic tweezers, Proc. Natl. Acad. Sci. U. S. A. 116 (2019) 84–89.
[126] M. Tanter, J.L. Thomas, M. Fink, Time reversal and the inverse filter, J. Acoust. Soc. Am. 108 (2000) 223–234.
[127] K. Melde, E. Choi, Z. Wu, S. Palagi, T. Qiu, P. Fischer, Acoustic Fabrication via the Assembly and Fusion of Particles, Adv. Mater. 30 (2018) 1704507.
[128] S. Jiménez-Gambín, N. Jiménez, J.M. Benlloch, F. Camarena, Holograms to Focus Arbitrary Ultrasonic Fields through the Skull, Phys. Rev. Appl. 12 (2019) 014016.
[129] Z. Ma, A.W. Holle, K. Melde, T. Qiu, K. Poeppel, V.M. Kadiri, P. Fischer, Acoustic Holographic Cell Patterning in a Biocompatible Hydrogel, Adv. Mater. 32 (2020) 1904181.
[130] S. Jiménez-Gambín, N. Jiménez, J.M. Benlloch, F. Camarena, Generating Bessel beams with broad depth-of-field by using phase-only acoustic holograms, Sci. Rep. 9 (2019) 1–13.
[131] K. Melde, H. Kremer, M. Shi, S. Seneca, C. Frey, I. Platzman, C. Degel, D. Schmitt, B. Schölkopf, P. Fischer, Compact holographic sound fields enable rapid one-step assembly of matter in 3D, Sci Adv 9 (2023) eadf6182.
[132] N. Jiménez, R. Picó, V. Sánchez-Morcillo, V. Romero-García, L.M. García-Raffi, K. Staliunas, Formation of high-order acoustic Bessel beams by spiral diffraction gratings, Phys. Rev. E 94 (2016) 053004.
[133] T. Wang, M. Ke, W. Li, Q. Yang, C. Qiu, Z. Liu, Particle manipulation with acoustic vortex beam induced by a brass plate with spiral shape structure, Appl. Phys. Lett. 109 (2016) 123506.
[134] N. Jiménez, V. Romero-García, L.M. García-Raffi, F. Camarena, K. Staliunas, Sharp acoustic vortex focusing by Fresnel-spiral zone plates, Appl. Phys. Lett. 112 (2018) 204101.
[135] X. Jiang, Y. Li, B. Liang, J.-C. Cheng, L. Zhang, Convert Acoustic Resonances to Orbital Angular Momentum, Phys. Rev. Lett. 117 (2016) 034301.
[136] V. Chan, A. Perlas, Basics of Ultrasound Imaging, Atlas of Ultrasound-Guided Procedures in Interventional Pain Management (2011) 13–19.
[137] J. Deprez, G. Lajoinie, Y. Engelen, S.C. De Smedt, I. Lentacker, Opening doors with ultrasound and microbubbles: Beating biological barriers to promote drug delivery, Adv. Drug Deliv. Rev. 172 (2021) 9–36.
[138] L. Tu, Z. Liao, Z. Luo, Y.-L. Wu, A. Herrmann, S. Huo, Ultrasound-controlled drug release and drug activation for cancer therapy, Explorationen 1 (2021) 20210023.
[139] W. Poon, B.R. Kingston, B. Ouyang, W. Ngo, W.C.W. Chan, A framework for designing delivery systems, Nat. Nanotechnol. 15 (2020) 819–829.
[140] M.J. Mitchell, M.M. Billingsley, R.M. Haley, M.E. Wechsler, N.A. Peppas, R. Langer, Engineering precision nanoparticles for drug delivery, Nat. Rev. Drug Discov. 20 (2021) 101–124.
[141] L. Guerassimoff, M. Ferrere, A. Bossion, J. Nicolas, Stimuli-sensitive polymer prodrug nanocarriers by reversible-deactivation radical polymerization, Chem. Soc. Rev. 53 (2024) 6511–6567.
[142] S.V. Bhujbal, P. de Vos, S.P. Niclou, Drug and cell encapsulation: alternative delivery options for the treatment of malignant brain tumors, Adv. Drug Deliv. Rev. 67–68 (2014) 142–153.
[143] A. Upadhyay, S.V. Dalvi, Microbubble Formulations: Synthesis, Stability, Modeling and Biomedical Applications, Ultrasound Med. Biol. 45 (2019) 301–343.

[144] V.P. Torchilin, Recent advances with liposomes as pharmaceutical carriers, Nat. Rev. Drug Discov. 4 (2005) 145–160.
[145] A. Kavand, N. Anton, T. Vandamme, C.A. Serra, D. Chan-Seng, Synthesis and functionalization of hyperbranched polymers for targeted drug delivery, J. Control. Release 321 (2020) 285–311.
[146] S. Mura, J. Nicolas, P. Couvreur, Stimuli-responsive nanocarriers for drug delivery, Nat. Mater. 12 (2013) 991–1003.
[147] A. Bordat, T. Boissenot, J. Nicolas, N. Tsapis, Thermoresponsive polymer nanocarriers for biomedical applications, Adv. Drug Deliv. Rev. 138 (2019) 167–192.
[148] F. Sharifianjazi, M. Irani, A. Esmaeilkhanian, L. Bazli, M.S. Asl, H.W. Jang, S. Y. Kim, S. Ramakrishna, M. Shokouhimehr, R.S. Varma, Polymer incorporated magnetic nanoparticles: Applications for magnetoresponsive targeted drug delivery, Mater. Sci. Eng. B Solid State Mater. Adv. Technol. 272 (2021) 115358.
[149] N. Deirram, C. Zhang, S.S. Kermaniyan, A.P.R. Johnston, G.K. Such, pH-Responsive Polymer Nanoparticles for Drug Delivery, Macromol. Rapid Commun. 40 (2019) e1800917.
[150] D.M. El-Sherif, M.A. Wheatley, Development of a novel method for synthesis of a polymeric ultrasound contrast agent, J. Biomed. Mater. Res. A 66A (2003) 347–355.
[151] Oil-filled polymer microcapsules for ultrasound-mediated delivery of lipophilic drugs, J. Control. Release 133 (2009) 109–118.
[152] G.K. Kulsharova, M.B. Lee, F. Cheng, M. Haque, H. Choi, K. Kim, W.D. O'Brien Jr, G.L. Liu, In vitro and in vivo imaging of peptide-encapsulated polymer nanoparticles for cancer biomarker activated drug delivery, IEEE Trans. Nanobioscience 12 (2013) 304–310.
[153] D. Dheer, J. Nicolas, R. Shankar, Cathepsin-sensitive nanoscale drug delivery systems for cancer therapy and other diseases, Adv. Drug Deliv. Rev. 151–152 (2019) 130–151.
[154] R. Jiffrin, S.I.A. Razak, M.I. Jamaludin, A.S.A. Hamzah, M.A. Mazian, M.A. T. Jaya, M.Z. Nasrullah, M. Majrashi, A. Theyab, A.A. Aldarmahi, Z. Awan, M. M. Abdel-Daim, A.K. Azad, Electrospun Nanofiber Composites for Drug Delivery: A Review on Current Progresses, Polymers 14 (2022), https://doi.org/10.3390/polym14183725.
[155] M.K. Gaydhane, C.S. Sharma, S. Majumdar, Electrospun nanofibres in drug delivery: advances in controlled release strategies, RSC Adv. 13 (2023) 7312–7328.
[156] B. Song, C. Wu, J. Chang, Ultrasound-triggered dual-drug release from poly (lactic-co-glycolic acid)/mesoporous silica nanoparticles electrospun composite fibers, Regen Biomater 2 (2015) 229–237.
[157] H. Xia, Y. Zhao, R. Tong, Ultrasound-Mediated Polymeric Micelle Drug Delivery, Adv. Exp. Med. Biol. 880 (2016) 365–384.
[158] D.A. Davis, A. Hamilton, J. Yang, L.D. Cremar, D. Van Gough, S.L. Potisek, M. T. Ong, P.V. Braun, T.J. Martínez, S.R. White, J.S. Moore, N.R. Sottos, Force-induced activation of covalent bonds in mechanoresponsive polymeric materials, Nature 459 (2009) 68–72.
[159] K.M. Wiggins, J.N. Brantley, C.W. Bielawski, Polymer Mechanochemistry: Force Enabled Transformations, ACS Macro Lett. 1 (2012) 623–626.
[160] Y. Li, Y. Qin, Y. Shang, Y. Li, F. Liu, J. Luo, J. Zhu, X. Guo, Z. Wang, Y. Zhao, Mechano-Responsive Leapfrog Micelles Enable Interactive Apoptotic and Ferroptotic Cancer Therapy, Adv. Funct. Mater. 32 (2022) 2112000.
[161] T.M. Allen, P.R. Cullis, Liposomal drug delivery systems: from concept to clinical applications, Adv. Drug Deliv. Rev. 65 (2013) 36–48.
[162] S.-L. Huang, Liposomes in ultrasonic drug and gene delivery, Adv. Drug Deliv. Rev. 60 (2008) 1167–1176.
[163] I. Lentacker, S.C. De Smedt, N.N. Sanders, Drug loaded microbubble design for ultrasound triggered delivery, Soft Matter 5 (2009) 2161–2170.
[164] Y. Orita, S. Shimanuki, S. Okada, K. Nakamura, H. Nakamura, Y. Kitamoto, Y. Shimoyama, Y. Kurashina, Acoustic-responsive carbon dioxide-loaded liposomes for efficient drug release, Ultrason. Sonochem. 94 (2023) 106326.
[165] N. Sax, T. Kodama, Optimization of acoustic liposomes for improved in vitro and in vivo stability, Pharm. Res. 30 (2013) 218–224.
[166] K. Chetty, E. Stride, C.A. Sennoga, J.V. Hajnal, R.J. Eckersley, High-speed optical observations and simulation results of SonoVue microbubbles at low-pressure insonation, IEEE Trans. Ultrason. Ferroelectr. Freq. Control 55 (2008) 1333–1342.
[167] M.P. Purohit, K.S. Roy, Y. Xiang, B.J. Yu, M.M. Azadian, G. Muwanga, A.R. Hart, A.K. Taoube, D.G. Lopez, R.D. Airan, Acoustomechanically activatable liposomes for ultrasonic drug uncaging, bioRxiv (2023). DOI: 10.1101/2023.10.23.563690.
[168] Y. Xin, Q. Qi, Z. Mao, X. Zhan, PLGA nanoparticles introduction into mitoxantrone-loaded ultrasound-responsive liposomes: In vitro and in vivo investigations, Int. J. Pharm. 528 (2017) 47–54.
[169] N. Mignet, C. Marie, A. Delalande, S. Manta, M.-F. Bureau, G. Renault, D. Scherman, C. Pichon, Microbubbles for Nucleic Acid Delivery in Liver Using Mild Sonoporation, Methods Mol. Biol. 2019 (1943) 377–387.
[170] Biomaterials 34 (2013) 5423–5430.
[171] I. Lentacker, S.C. De Smedt, J. Demeester, V. Van Marck, M. Bracke, N.N. Sanders, Lipoplex-loaded microbubbles for gene delivery: A Trojan horse controlled by ultrasound, Adv. Funct. Mater. 17 (2007) 1910–1916.
[172] A.L. Klibanov, Preparation of targeted microbubbles: ultrasound contrast agents for molecular imaging, Med. Biol. Eng. Comput. 47 (2009) 875–882.
[173] T.A. Fritz, E.C. Unger, G. Sutherland, D. Sahn, Phase I Clinical Trials of MRX-115: A New Ultrasound Contrast Agent, Invest. Radiol. 32 (1997) 735.
[174] Determination of perfluorobutane in rat blood by automatic headspace capillary gas chromatography and selected ion monitoring mass spectrometry, J. Pharm. Biomed. Anal. 24 (2001) 487–494.
[175] Clinical experience with AF0150 (Imagent US), a new ultrasound contrast agent, Acad. Radiol. 5 (1998) S69–S71.
[176] M. Schneider, M. Arditi, M.-B. Barrau, J. Brochot, A. Broillet, R. Ventrone, F. Yan, BR1: A New Ultrasonographic Contrast Agent Based on Sulfur Hexafluoride-Filled Microbubbles, Invest. Radiol. 30 (1995) 451.
[177] J. Rich, Z. Tian, T.J. Huang, Sonoporation: Past, Present, and Future, Adv Mater Technol 7 (2022), https://doi.org/10.1002/admt.202100885.
[178] G. Shapiro, A.W. Wong, M. Bez, F. Yang, S. Tam, L. Even, D. Sheyn, S. Ben-David, W. Tawackoli, G. Pelled, K.W. Ferrara, D. Gazit, Multiparameter evaluation of in vivo gene delivery using ultrasound-guided, microbubble-enhanced sonoporation, J. Control. Release 223 (2016) 157–164.
[179] A. Delalande, C. Bastié, L. Pigeon, S. Manta, M. Lebertre, N. Mignet, P. Midoux, C. Pichon, Cationic gas-filled microbubbles for ultrasound-based nucleic acids delivery, Biosci. Rep. 37 (2017), https://doi.org/10.1042/BSR20160619.
[180] Int. J. Pharm. 414 (2011) 161–170.
[181] J. Tu, A.C.H. Yu, Ultrasound-Mediated Drug Delivery: Sonoporation Mechanisms, Biophysics, and Critical Factors, BME Front 2022 (2022) 9807347.
[182] Understanding ultrasound induced sonoporation, Definitions and underlying mechanisms, Adv. Drug Deliv. Rev. 72 (2014) 49–64.
[183] Mechanisms underlying sonoporation, Interaction between microbubbles and cells, Ultrason. Sonochem. 67 (2020) 105096.
[184] H. Chen, W. Kreider, A.A. Brayman, M.R. Bailey, T.J. Matula, Blood vessel deformations on microsecond time scales by ultrasonic cavitation, Phys. Rev. Lett. 106 (2011) 034301.
[185] W.M. Pardridge, The blood-brain barrier: Bottleneck in brain drug development, NeuroRx 2 (2005) 3–14.
[186] P. Mondou, S. Mériaux, F. Nageotte, J. Vappou, A. Novell, B. Larrat, State of the art on microbubble cavitation monitoring and feedback control for blood-brain-barrier opening using focused ultrasound, Phys. Med. Biol. 68 (2023), https://doi.org/10.1088/1361-6560/ace23e.
[187] L.H. Treat, N. McDannold, N. Vykhodtseva, Y. Zhang, K. Tam, K. Hynynen, Targeted delivery of doxorubicin to the rat brain at therapeutic levels using MRI-guided focused ultrasound, Int. J. Cancer 121 (2007) 901–907.
[188] G. Shakya, M. Cattaneo, G. Guerriero, A. Prasanna, S. Fiorini, O. Supponen, Ultrasound-responsive microbubbles and nanodroplets: A pathway to targeted drug delivery, Adv. Drug Deliv. Rev. 206 (2024) 115178.
[189] W. Zhang, Y. Shi, S. Abd Shukor, A. Vijayakumaran, S. Vlatakis, M. Wright, M. Thanou, Phase-shift nanodroplets as an emerging sonoresponsive nanomaterial for imaging and drug delivery applications, Nanoscale 14 (2022) 2943–2965.
[190] M.A. Borden, G. Shakya, A. Upadhyay, K.-H. Song, Acoustic Nanodrops for Biomedical Applications, Curr. Opin. Colloid Interface Sci. 50 (2020), https://doi.org/10.1016/j.cocis.2020.08.008.
[191] A.L.Y. Kee, B.M. Teo, Biomedical applications of acoustically responsive phase shift nanodroplets: Current status and future directions, Ultrason. Sonochem. 56 (2019) 37–45.
[192] R. Chattaraj, P. Mohan, J.D. Besmer, A.P. Goodwin, Selective Vaporization of Superheated Nanodroplets for Rapid, Sensitive, Acoustic Biosensing, Adv. Healthc. Mater. 4 (2015) 1790–1795.
[193] H. Lea-Banks, M.A. O'Reilly, K. Hynynen, Ultrasound-responsive droplets for therapy: A review, J. Control. Release 293 (2019) 144–154.
[194] C.C. Chen, P.S. Sheeran, S.-Y. Wu, O.O. Olumolade, P.A. Dayton, E.E. Konofagou, Targeted drug delivery with focused ultrasound-induced blood-brain barrier opening using acoustically-activated nanodroplets, J. Control. Release 172 (2013) 795–804.
[195] C.J. Brambila, J. Lux, R.F. Mattrey, D. Boyd, M.A. Borden, C. de Gracia Lux, Bubble Inflation Using Phase-Change Perfluorocarbon Nanodroplets as a Strategy for Enhanced Ultrasound Imaging and Therapy, Langmuir 36 (2020) 2954–2965.
[196] P. Sontum, S. Kvåle, A.J. Healey, R. Skurtveit, R. Watanabe, M. Matsumura, J. Østensen, Acoustic Cluster Therapy (ACT)–A novel concept for ultrasound mediated, targeted drug delivery, Int. J. Pharm. 495 (2015) 1019–1027.
[197] D. Yang, Q. Chen, M. Zhang, G. Feng, D. Sun, L. Lin, X. Jing, Drug-loaded acoustic nanodroplet for dual-imaging guided highly efficient chemotherapy against nasopharyngeal carcinoma, Int. J. Nanomedicine 17 (2022) 4879–4894.
[198] A. Honari, D.A. Merillat, A. Bellary, M. Ghaderi, S.R. Sirsi, Improving release of liposome-encapsulated drugs with focused ultrasound and vaporizable droplet-liposome nanoclusters, Pharmaceutics 13 (2021) 609.
[199] C.-P. Spatarelu, S. Jandhyala, G.P. Luke, Dual-drug loaded ultrasound-responsive nanodroplets for on-demand combination chemotherapy, Ultrasonics 133 (2023) 107056.
[200] Y.-S. Chen, Y. Zhao, C. Beinat, A. Zlitni, E.-C. Hsu, D.-H. Chen, F. Achterberg, H. Wang, T. Stoyanova, J. Dionne, S.S. Gambhir, Ultra-high-frequency radio-frequency acoustic molecular imaging with saline nanodroplets in living subjects, Nat. Nanotechnol. 16 (2021) 717–724.
[201] T. Luo, S. Liu, R. Zhou, C. Zhang, D. Chen, Y. Zhan, Q. Hu, X. He, Y. Xie, Z. Huan, W. Gao, R. Li, G. Yuan, Y. Wang, W. Zhou, Contactless acoustic tweezer for droplet manipulation on superhydrophobic surfaces, Lab Chip 23 (2023) 3989–4001.
[202] Y. Vitry, S. Dorbolo, J. Vermant, B. Scheid, Controlling the lifetime of antibubbles, Adv. Colloid Interface Sci. 270 (2019) 73–86.
[203] S. Dorbolo, E. Reyssat, N. Vandewalle, D. Quéré, Aging of an antibubble, EPL 69 (2005) 966–970.
[204] A.T. Poortinga, Long-lived antibubbles: stable antibubbles through Pickering stabilization, Langmuir 27 (2011) 2138–2141.
[205] A.T. Poortinga, Micron-sized antibubbles with tunable stability, Colloids Surf. A Physicochem. Eng. Asp. 419 (2013) 15–20.

[206] S. Kotopoulis, C. Lam, R. Haugse, S. Snipstad, E. Murvold, T. Jouleh, S. Berg, R. Hansen, M. Popa, E. Mc Cormack, O.H. Gilja, A. Poortinga, Formulation and characterisation of drug-loaded antibubbles for image-guided and ultrasound-triggered drug delivery, Ultrason. Sonochem. 85 (2022) 105986.
[207] N. Moreno-Gomez, A.G. Athanassiadis, A.T. Poortinga, P. Fischer, Antibubbles Enable Tunable Payload Release with Low-Intensity Ultrasound, Adv. Mater. 35 (2023) e2305296.
[208] N. Kudo, R. Uzbekov, R. Matsumoto, R.-I. Shimizu, C.S. Carlson, N. Anderton, A. Deroubaix, C. Penny, A.T. Poortinga, D.M. Rubin, A. Bouakaz, M. Postema, Asymmetric oscillations of endoskeletal antibubbles, Jpn. J. Appl. Phys. 59 (2020) SKKE02.
[209] R. Zia, A.T. Poortinga, A. Nazir, M. Ayyash, C.F. van Nostrum, Preparation of acid-responsive antibubbles from CaCO-based Pickering emulsions, J. Colloid Interface Sci. 652 (2023) 2054–2065.
[210] R. Zia, A.T. Poortinga, A. Nazir, S. Aburuz, C.F. van Nostrum, Triple-Emulsion-Based Antibubbles: A Step Forward in Fabricating Novel Multi-Drug Delivery Systems, Pharmaceutics 15 (2023), https://doi.org/10.3390/pharmaceutics15122757.
[211] U. Dristant, K. Mukherjee, S. Saha, D. Maity, An Overview of Polymeric Nanoparticles-Based Drug Delivery System in Cancer Treatment, Technol. Cancer Res. Treat. 22 (2023) 15330338231152083.
[212] M.A. Beach, U. Nayanathara, Y. Gao, C. Zhang, Y. Xiong, Y. Wang, G.K. Such, Polymeric Nanoparticles for Drug Delivery, Chem. Rev. 124 (2024) 5505–5616.
[213] K. Wieszczycka, K. Staszak, M.J. Woźniak-Budych, J. Litowczenko, B. M. Maciejewska, S. Jurga, Surface functionalization – The way for advanced applications of smart materials, Coord. Chem. Rev. 436 (2021) 213846.
[214] P. Wei, E.J. Cornel, J. Du, Ultrasound-responsive polymer-based drug delivery systems, Drug Deliv, Transl. Res. 11 (2021) 1323–1339.
[215] H.B. Haroon, A.C. Hunter, Z.S. Farhangrazi, S.M. Moghimi, A brief history of long circulating nanoparticles, Adv. Drug Deliv. Rev. 188 (2022) 114396.
[216] C. Fornaguera, C. Castells-Sala, S. Borrós, Unraveling Polymeric Nanoparticles Cell Uptake Pathways: Two Decades Working to Understand Nanoparticles Journey to Improve Gene Therapy, Adv. Exp. Med. Biol. 1288 (2020) 117–138.
[217] E. Stride, T. Segers, G. Lajoinie, S. Cherkaoui, T. Bettinger, M. Versluis, M. Borden, Microbubble Agents: New Directions, Ultrasound Med. Biol. 46 (2020) 1326–1343.
[218] S.-L. Huang, R.C. MacDonald, Acoustically active liposomes for drug encapsulation and ultrasound-triggered release, Biochim. Biophys. Acta 1665 (2004) 134–141.
[219] K.E. Hitchcock, D.N. Caudell, J.T. Sutton, M.E. Klegerman, D. Vela, G.J. Pyne-Geithman, T. Abruzzo, P.E.P. Cyr, Y.-J. Geng, D.D. McPherson, C.K. Holland, Ultrasound-enhanced delivery of targeted echogenic liposomes in a novel ex vivo mouse aorta model, J. Control. Release 144 (2010) 288–295.
[220] S. Paul, R. Nahire, S. Mallik, K. Sarkar, Encapsulated microbubbles and echogenic liposomes for contrast ultrasound imaging and targeted drug delivery, Comput. Mech. 53 (2014) 413–435.
[221] K.D. Buchanan, S. Huang, H. Kim, R.C. Macdonald, D.D. McPherson, Echogenic liposome compositions for increased retention of ultrasound reflectivity at physiologic temperature, J. Pharm. Sci. 97 (2008) 2242–2249.
[222] D. Park, H.C. Jung, J. Park, S. Bae, U. Shin, S.W. Kim, C.W. Kim, Y.H. Lee, J. Seo, Synthesis of echogenic liposomes for sonoporation, Micro, Nano Lett. 17 (2022) 276–285.
[223] R. Nahire, R. Hossain, R. Patel, S. Paul, V. Meghnani, A.H. Ambre, K.N. Gange, K. S. Katti, E. Leclerc, D.K. Srivastava, K. Sarkar, S. Mallik, pH-triggered echogenicity and contents release from liposomes, Mol. Pharm. 11 (2014) 4059–4068.
[224] A. Yudina, M. de Smet, M. Lepetit-Coiffé, S. Langereis, L. Van Ruijssevelt, P. Smirnov, V. Bouchaud, P. Voisin, H. Grüll, C.T.W. Moonen, Ultrasound-mediated intracellular drug delivery using microbubbles and temperature-sensitive liposomes, J. Control. Release 155 (2011) 442–448.
[225] N. Rajankar, M. Aalhate, S. Mahajan, I. Maji, U. Gupta, R. Nair, P. Paul, P. K. Singh, Unveiling multifaceted avenues of echogenic liposomes: Properties, preparation, and potential applications, J. Drug Deliv. Sci. Technol. 99 (2024) 105931.
[226] H. Lin, J. Chen, C. Chen, A novel technology: microfluidic devices for microbubble ultrasound contrast agent generation, Med. Biol. Eng. Comput. 54 (2016) 1317–1330.
[227] Q. Gong, X. Gao, W. Liu, T. Hong, C. Chen, Drug-Loaded Microbubbles Combined with Ultrasound for Thrombolysis and Malignant Tumor Therapy, Biomed Res. Int. 2019 (2019) 6792465.
[228] J.R. Lindner, Microbubbles in medical imaging: current applications and future directions, Nat. Rev. Drug Discov. 3 (2004) 527–532.
[229] E. Stride, Magnetic nanodroplets for targeted drug delivery, Ultrasound Med. Biol. 45 (2019) S49.
[230] I. Beekers, S.A.G. Langeveld, B. Meijlink, A.F.W. van der Steen, N. de Jong, M. D. Verweij, K. Kooiman, Internalization of targeted microbubbles by endothelial cells and drug delivery by pores and tunnels, J. Control. Release 347 (2022) 460–475.
[231] N. Rapoport, Phase-shift, stimuli-responsive perfluorocarbon nanodroplets for drug delivery to cancer, Wiley Interdiscip. Rev. Nanomed. Nanobiotechnol. 4 (2012) 492–510.
[232] K. Wilson, K. Homan, S. Emelianov, Biomedical photoacoustics beyond thermal expansion using triggered nanodroplet vaporization for contrast-enhanced imaging, Nat. Commun. 3 (2012) 618.
[233] S. Ferri, Q. Wu, A. De Grazia, A. Polydorou, J.P. May, E. Stride, N.D. Evans, D. Carugo, Tailoring the size of ultrasound responsive lipid-shelled nanodroplets by varying production parameters and environmental conditions, Ultrason. Sonochem. 73 (2021) 105482.
[234] A. Kumawat, B. Saini, C. Ghoroi, Nanodroplets Engineered with Folate Carbon Dots for Enhanced Cancer Cell Uptake toward Theranostic Application, ACS Appl Bio Mater (2024), https://doi.org/10.1021/acsabm.4c00633.
[235] A. Ozcelik, J. Rufo, F. Guo, Y. Gu, P. Li, J. Lata, T.J. Huang, Acoustic tweezers for the life sciences, Nat. Methods 15 (2018) 1021–1028.
[236] Q.B. Huynh, H.Q. Pham, N.T. Nguyen, T.Q. Le, V. Van Toi, Modeling of acoustic tweezers for the manipulation in biological media, in: IFMBE Proceedings, Springer Singapore, Singapore, 2020: pp. 127–135.
[237] M. Abkarian, A.B. Subramaniam, S.-H. Kim, R.J. Larsen, S.-M. Yang, H.A. Stone, Dissolution Arrest and Stability of Particle-Covered Bubbles, Phys. Rev. Lett. 99 (2007) 188301.
[238] H.X. Cao, D. Jung, H.-S. Lee, V.D. Nguyen, E. Choi, B. Kang, J.-O. Park, C.-S. Kim, Holographic Acoustic Tweezers for 5-DoF Manipulation of Nanocarrier Clusters toward Targeted Drug Delivery, Pharmaceutics 14 (2022), https://doi.org/10.3390/pharmaceutics14071490.
[239] Y. Li, M. Guo, G. Guo, Q. Ma, Transdermal drug delivery mediated by acoustic vortex beam, Ultrasonics 140 (2024) 107304.
[240] W.-C. Lo, C.-H. Fan, Y.-J. Ho, C.-W. Lin, C.-K. Yeh, Tornado-inspired acoustic vortex tweezer for trapping and manipulating microbubbles, Proc. Natl. Acad. Sci. U. S. A. 118 (2021), https://doi.org/10.1073/pnas.2023188118.
[241] Y. Li, C. Lee, R. Chen, Q. Zhou, K.K. Shung, A feasibility study of applications of single beam acoustic tweezers, Appl. Phys. Lett. 105 (2014) 173701.
[242] H. Wen, H. Jung, X. Li, Drug Delivery Approaches in Addressing Clinical Pharmacology-Related Issues: Opportunities and Challenges, AAPS J 17 (2015) 1327–1340.